

อนุภาคระดับนาโนเมตรของแม่เหล็กทำให้เสถียรด้วยพอลิเมอร์คอนจูเกตกับเอนไซม์สำหรับการแยกและ  
การตรวจวัดเชื้อมิวแทนส์สเตรปโตคอคไค



นางสาวเอมวิภา วิทยาประสิทธิ์

จุฬาลงกรณ์มหาวิทยาลัย

CHULALONGKORN UNIVERSITY

บทคัดย่อและแฟ้มข้อมูลฉบับเต็มของวิทยานิพนธ์ตั้งแต่ปีการศึกษา 2554 ที่ให้บริการในคลังปัญญาจุฬาฯ (CUIR)  
เป็นแฟ้มข้อมูลของนิสิตเจ้าของวิทยานิพนธ์ ที่ส่งผ่านทางบัณฑิตวิทยาลัย

The abstract and full text of theses from the academic year 2011 in Chulalongkorn University Intellectual Repository (CUIR)  
are the thesis authors' files submitted through the University Graduate School.

วิทยานิพนธ์นี้เป็นส่วนหนึ่งของการศึกษาตามหลักสูตรปริญญาวิทยาศาสตรมหาบัณฑิต

สาขาวิชาปิโตรเคมีและวิทยาศาสตร์พอลิเมอร์

คณะวิทยาศาสตร์ จุฬาลงกรณ์มหาวิทยาลัย

ปีการศึกษา 2558

ลิขสิทธิ์ของจุฬาลงกรณ์มหาวิทยาลัย

MAGNETIC NANOPARTICLES STABILIZED WITH ENZYME-  
CONJUGATED POLYMER FOR SEPARATION AND DETECTION OF MUTANS STREPTOCOCCI

Miss Aemvika Vittayaprasit



A Thesis Submitted in Partial Fulfillment of the Requirements  
for the Degree of Master of Science Program in Petrochemistry and Polymer Science

Faculty of Science

Chulalongkorn University

Academic Year 2015

Copyright of Chulalongkorn University

Thesis Title	MAGNETIC NANOPARTICLES STABILIZED WITH ENZYME-CONJUGATED POLYMER FOR SEPARATION AND DETECTION OF MUTANS STREPTOCOCCI
By	Miss Aemvika Vittayaprasit
Field of Study	Petrochemistry and Polymer Science
Thesis Advisor	Associate Professor Voravee Hoven, Ph.D.
Thesis Co-Advisor	Panida Thanyasrisung, Ph.D.

---

Accepted by the Faculty of Science, Chulalongkorn University in Partial Fulfillment of the Requirements for the Master's Degree

.....Dean of the Faculty of Science  
(Associate Professor Polkit Sangvanich, Ph.D.)

THESIS COMMITTEE

.....Chairman  
(Professor Pattarapan Prasassarakich, Ph.D.)

.....Thesis Advisor  
(Associate Professor Voravee Hoven, Ph.D.)

.....Thesis Co-Advisor  
(Panida Thanyasrisung, Ph.D.)

.....Examiner  
(Assistant Professor Varawut Tangpasuthadol, Ph.D.)

.....External Examiner  
(Duangporn Polpanich, Ph.D.)

เอมวีกา วิทยาประสิทธิ์ : อนุภาคระดับนาโนเมตรของแม่เหล็กทำให้เสถียรด้วยพอลิเมอร์  
 คอนจูเกตกับเอนไซม์สำหรับการแยกและการตรวจวัดเชื้อมีวแทนส์สเตรปโตคอคโค  
 (MAGNETIC NANOPARTICLES STABILIZED WITH ENZYME-CONJUGATED  
 POLYMER FOR SEPARATION AND DETECTION OF MUTANS STREPTOCOCCI) อ.  
 ที่ปริภษาวิทยานิพนธ์หลัก: รศ. ดร.วรวิร์ โสเวน, อ.ที่ปริภษาวิทยานิพนธ์ร่วม: ดร.พนิดา  
 ัญญศรีสังข์, 51 หน้า.

งานวิจัยนี้มีเป้าหมายที่จะพัฒนาวิธีทดสอบที่ง่ายและมีประสิทธิภาพสำหรับการตรวจวัด  
 ปริมาณกลุ่มเชื้อมีวแทนส์สเตรปโตคอคโคอาศัยกระบวนการแยกด้วยแม่เหล็กร่วมกับการกรองแบบ  
 เลือกว่านเมมเบรน อนุภาคแม่เหล็กนาโนสังเคราะห์โดยกระบวนการโซลโวเทอร์มอลถูกกราฟต์ด้วย  
 พอลิอะคริลิกแอซิดซึ่งมีหมู่คาร์บอกซิลที่พร้อมคอนจูเกตกับชิ้นส่วนที่จับกับผนังเซลล์ (CWBD) ของ  
 เอนไซม์ออโตมิวตาโนไลซิน ซึ่งเป็นเอนไซม์ที่มีความจำเพาะเจาะจงกับกลุ่มเชื้อมีวแทนส์สเตรปโตคอค  
 โค สามารถพิสูจน์เอกลักษณ์ของอนุภาคแม่เหล็กนาโนที่ถูกดัดแปรหมู่ฟังก์ชันด้วยเทคนิค XRD, FT-  
 IR, TEM, DLS และ TGA การทดสอบการจับกับแบคทีเรียทำได้โดยการผสมอนุภาคแม่เหล็กนาโนที่  
 คอนจูเกตกับ CWBD กับแบคทีเรีย จากนั้นจึงนำมาแยกออกจากสารละลายโดยอาศัยแม่เหล็ก  
 ภายนอก อนุภาคแม่เหล็กนาโนที่คอนจูเกตกับ CWBD และจับกับแบคทีเรียที่แยกได้จะถูกนำไปทำ  
 เป็นสารละลายก่อนกรองสุญญากาศผ่านไนโตรเซลลูโลสเมมเบรนที่มีขนาดของรู 0.8 ไมโครเมตร  
 ความเข้มข้นของจุดที่เกิดบนเมมเบรนแปรผันตรงตามความเข้มข้นของแบคทีเรียเป้าหมายทั้งสองชนิด  
 คือ *S. mutans* and *S. sobrinus* ในช่วงความเข้มข้น  $1 \times 10^2$  -  $1 \times 10^7$  CFU/mL อนุภาคแม่เหล็กนา  
 โนที่คอนจูเกตกับ CWBD มีความจำเพาะกับ *S. mutans* และ *S. sobrinus* ที่มีประสิทธิภาพในการจับ  
 77 และ 69% ตามลำดับ มากกว่ากับแบคทีเรียที่ไม่ได้เป็นเป้าหมายคือ *S. salivarius* และ  
*S. sanguinis* ที่มีประสิทธิภาพในการจับ 15 และ 38% ตามลำดับ อาศัยสมบัติการมีแอกติวิตี  
 เหมือนกับเปอร์ออกซิเดสของอนุภาคแม่เหล็กนาโน การเติม TMB และ  $H_2O_2$  ลงบนจุดบนแผ่นเมม  
 เบรนช่วยขยายสัญญาณในการตรวจวัดและเพิ่มขีดจำกัดการตรวจวัดของ *S. mutans* จาก  $2 \times 10^1$   
 เป็น 8 CFU/mL จากกระบวนการวิเคราะห์ที่ทำได้ง่าย มีความไวและความจำเพาะเจาะจงสูง และ  
 การให้สัญญาณอย่างรวดเร็ว การวิเคราะห์การเกิดสีโดยใช้อนุภาคแม่เหล็กนาโนที่คอนจูเกตกับ  
 CWBD นี้ จัดเป็นเป็นเครื่องมือตรวจวัดกลุ่มเชื้อมีวแทนส์สเตรปโตคอคโคที่มีความรวดเร็วและมี  
 ศักยภาพที่น่าจะสามารถนำมาปรับใช้ทางคลินิกได้

สาขาวิชา ปีโตรเคมีและวิทยาศาสตร์พอลิเมอร์ ลายมือชื่อนิสิต .....

ปีการศึกษา 2558

ลายมือชื่อ อ.ที่ปรึกษาหลัก .....

ลายมือชื่อ อ.ที่ปรึกษาร่วม .....

# # 5672248123 : MAJOR PETROCHEMISTRY AND POLYMER SCIENCE

KEYWORDS: MAGNETIC NANOPARTICLES / SELECTIVE FILTRATION

AEMVIKA VITTAYAPRASIT: MAGNETIC NANOPARTICLES STABILIZED WITH ENZYME-CONJUGATED POLYMER FOR SEPARATION AND DETECTION OF MUTANS STREPTOCOCCI. ADVISOR: ASSOC. PROF. VORAVEE HOVEN, Ph.D., CO-ADVISOR: PANIDA THANYASRISUNG, Ph.D., 51 pp.

This research aims to develop a simple, yet effective assay for mutans streptococci (*Streptococcus mutans* and *Streptococcus sobrinus*) detection based on a combination of magnetic separation and selective filtration. Magnetic nanoparticles (MNPs) synthesized by solvothermal process were first grafted with poly(acrylic acid) (PAA) bearing active carboxyl groups, readily available for conjugation with cell wall binding domain (CWBD) of automutanolysin that is specific to mutans streptococci. The functionalized MNPs were characterized by XRD, FT-IR, TEM, DLS, and TGA. To determine the bacteria binding, the CWBD-conjugated MNPs were mixed with bacteria solution and then isolated by a magnet. The isolated bacteria bound CWBD-conjugated MNPs were re-suspended and then passed through a membrane (pore size 0.8  $\mu\text{m}$ ) by vacuum filtration. The intensity of the colored spots on the membrane was found to increase linearly with concentration of both targeted bacteria, Mutans streptococci in a concentration range of  $1 \times 10^2$  -  $1 \times 10^7$  CFU/mL. The CWBD-conjugated MNPs were more specific to *S. mutans* and *S. sobrinus* with capture efficiency of 77 and 69%, respectively than non-targeted bacteria, *S. salivarius* and *S. sanguinis* with capture efficiency of 15 and 38%, respectively. Taking a benefit of peroxidase-like activity of MNPs, an addition of TMB and  $\text{H}_2\text{O}_2$  on the spots on the membrane could amplify the signal and thus improve the detection limit of the assay for *S. mutans* detection from 20 to 8 CFU/mL. With the ease of operation, high sensitivity and specificity as well as the quick response time, the colorimetric assay employing CWBD-conjugated MNPs is a promising detection tool for mutans streptococci detection that may be implemented in clinical setting.

Field of Study: Petrochemistry and Student's Signature .....

Polymer Science Advisor's Signature .....

Academic Year: 2015 Co-Advisor's Signature .....

## ACKNOWLEDGEMENTS

First and foremost I wish to express my sincere and deep gratitude to my advisor and coadvisor, Associate Professor Dr. Voravee Hoven and Dr. Panida Thanyasrisung for her thoughtful guidance, steady encouragement and support, and consistent generosity and consideration. Working with her has been the best course of my study.

I sincerely thank to Professor Dr.Pattarapan Prasassarakich, Assistant Professor Dr.Varawut Tangpasuthadol and Dr. Duangporn Ponpanich for acting as the chairman and examiner of my thesis committee, respectively and for their valuable constructive comments and suggestions. The authors are grateful to the Department of Chemistry, Faculty of Science, Burapa University, for providing the TEM analysis.

Financial support for this work was provided by the Thailand Research Fund (DBG5580003) and Ratchadapiseksomphot Endowment Fund under Outstanding Research Performance Program (GF\_58\_08\_23\_01).

Furthermore, I would like to thank members of Organic Synthesis Research Unit (OSRU) Department of Chemistry and Department of Microbiology and Research Unit on Oral Microbiology and Immunology, Faculty of Dentistry for their friendliness, helpful discussions, and encouragements.

Finally, I also wish to especially thank my beloved family for their love, encouragement and support throughout my entire study.

## CONTENTS

	Page
THAI ABSTRACT.....	iv
ENGLISH ABSTRACT.....	v
ACKNOWLEDGEMENTS .....	vi
CONTENTS.....	vii
LIST OF FIGURES.....	x
LIST OF TABLES .....	xii
LIST OF ABBREVIATION.....	xiii
CHAPTER I INTRODUCTION.....	1
1.1 Inroduction .....	1
1.2 Objectives.....	15
1.3 Scope of investigation.....	15
CHAPTER II EXPERIMENTAL .....	16
2.1 Materials.....	16
2.2 Equipments .....	16
2.2.1 Fourier Transform-Infrared Spectroscopy (FT-IR).....	16
2.2.2 Thermogravimetric Analysis (TGA).....	16
2.2.3 Transmission Electron Microscopy (TEM) .....	17
2.2.4 X-ray Diffraction (XRD).....	17
2.2.5 Dynamic Light Scattering (DLS) .....	17
2.2.6 Scanner .....	17
2.3 Experimental Procedure.....	18
2.3.1 Preparation of Cell Wall Binding Domain of Automutanolysin.....	18

	Page
2.3.2 Synthesis of MNPs by Solvothermal Method.....	18
2.3.3 Preparation of PAA-grafted MNPs.....	19
2.3.4 Immobilization of CWBD on PAA-grafted MNPs.....	20
2.3.5 Oxidative Catalytic Property of MNPs. ....	21
2.3.6 Bacterial Culturing.....	21
2.3.7 Determination of Bacteria Capturing by CWBD-conjugated MNPs .....	22
CHAPTER III RESULTS AND DISCUSSION .....	24
3.1 Preparation and characterization of PAA-grafted MNPs and CWBD- conjugated MNPs .....	24
3.2 Selection of Filter Membranes Suitable for Selective Filtration Assay.....	29
3.3 Determination of Peroxidase-like Activity of MNPs .....	31
3.4 Determination of Bacteria Binding of CWBD-PAA-MNPs .....	33
3.5 Determination of Bacteria Capture Efficiency of CWBD-conjugated MNPs.....	36
CHAPTER V CONCLUSION AND SUGGESTIONS .....	40
REFERENCES.....	43
VITA .....	51



## LIST OF FIGURES

<b>Figure 1.1</b> Magnetic separation and colorimetric detection process for the <i>S. aureus</i> sensing using antibody/AuNP/MNPs and selective filtration method.....	4
<b>Figure 1.2</b> Schematic diagram of a selective filtration method based on a monoclonal antibody (MAb)-conjugated magnetic nanoparticle (MNP) for the rapid and sensitive detection of <i>L. monocytogenes</i> [12]. .....	5
<b>Figure 1.3</b> Generally accepted mechanism for RAFT polymerization.....	7
<b>Figure 1.4</b> TMB can act as a hydrogen donor for the reduction of hydrogen peroxide to water by MNPs nanocomposites, the resulting diimine causes the solution to take on a blue color.....	11
<b>Figure 1.5</b> Schematic illustration of the MNP-based colorimetric detection using label-free DNA aptamers and TMB.....	13
<b>Figure 1.6</b> Schematic representation of colorimetric detection of mutans streptococci with MNPs grafted with PAA and immobilized with CWBD of Automutanolysin.....	14
<b>Figure 2.1</b> Preparation of PAA-grafted MNPs via surface-initiated RAFT polymerization.....	20
<b>Figure 2.2</b> Conjugation of CWBD with PAA-grafted MNPs via EDC/NHS coupling. ....	20
<b>Figure 2.3</b> Magnetic separation and selective filtration process of mutans streptococci using CWBD-conjugated MNPs.....	23
<b>Figure 3.1</b> XRD pattern of bare MNPs nanoparticles prepared by solvothermal method.....	24
<b>Figure 3.2</b> FT-IR spectra of MNPs: (a) unmodified, (b) grafted with PAA and (c) conjugated with CWBD.....	25

<b>Figure 3.3</b> TEM micrographs of (a) bare MNPs, (b) PAA-grafted MNPs, and (c) CWBD-conjugated MNPs (scale bar 1 $\mu$ m (top) and 0.5 $\mu$ m (bottom), respectively). ....	26
<b>Figure 3.4</b> TGA (under N <sub>2</sub> ) curves of (a) unmodified MNPs, (b) PAA-grafted MNPs, and (c) CWBD-conjugated MNPs analyzed with a heating rate of 20 $^{\circ}$ C/min.....	28
<b>Figure 3.5</b> <sup>1</sup> H NMR spectrum of PAA in D <sub>2</sub> O .....	29
<b>Figure 3.6</b> The peroxidase-like activity of MNPs to catalyze the color reaction of TMB in the presence of H <sub>2</sub> O <sub>2</sub> which was varied as a function of the amount of (a) TMB substrate, (b) MNPs, and (c) H <sub>2</sub> O <sub>2</sub> .....	33
<b>Figure 3.7</b> Linear relationship between log (CFU/mL) and intensity both (a) before and (b) after signal amplification in the presence of TMB/H <sub>2</sub> O <sub>2</sub> for <i>S. mutans</i> .....	35
<b>Figure 3.8</b> Linear relationship between log (CFU/mL) and intensity both before (a) and after (b) signal amplification in the presence of TMB/H <sub>2</sub> O <sub>2</sub> for <i>S. sobrinus</i> .....	36
<b>Figure 3.9</b> Colonies of (a) <i>S. mutans</i> , (b) <i>S. sobrinus</i> , (c) <i>S. salivarius</i> , and (d) <i>S. sanguinis</i> before and after the addition of CWBD-conjugated MNPs.....	37
<b>Figure 3.10</b> Determination of specificity of the CWBD-conjugated MNPs against all bacteria.....	39

## LIST OF TABLES

<b>Table 2.1</b> Various the quantities of TMB, H <sub>2</sub> O <sub>2</sub> and MNPs for optimization.....	21
<b>Table 3.1</b> Average size and zeta potential of MNPs measured by DLS.....	27
<b>Table 3.2</b> Color signal and its corresponding intensity of the spot on the nitrocellulose membrane having varied pore size after filtering MNPs, PAA-grafted MNPs, CWBD-conjugated MNPs both before and after bacteria capturing.....	31
<b>Table A.1</b> Amino acid composition of automutanolysin.....	49



## LIST OF ABBREVIATION

ACVA	: 4,4-Azobis(4-cyanovaleric acid)
APTES	: 3-Aminopropyltriethoxysilane
CPD	: 4-Cyano-4-(phenylcarbonothio) pentanoic acid
CWBD	: Cell wall binding domain
DCC	: <i>N,N'</i> -dicyclohexylcarbodiimide
DLS	: Dynamic Light Scattering
DMAP	: 4-(dimethylamino)pyridine
DMF	: Dimethylformamide
EDC	: 1-Ethyl-3-(3dimethylaminopropyl)carbodiimide
FTIR	: Fourier Transform-Infrared Spectroscopy
MNPs	: Magnetic nanoparticles
NHS	: <i>N</i> -hydroxysuccinimide
PAA	: Poly(acrylic acid)
RAFT	: Reversible addition-fragmentation chain transfer
TEM	: Transmission Electron Microscopy
TGA	: Thermogravimetric Analysis
TMB	: 3,3',5,5'-Tetramethylbenzidine
XRD	: X-ray Diffraction

# CHAPTER I

## INTRODUCTION

### 1.1 Introduction

Dental caries is not life-threatening disease but it has association with systemic diseases such as respiratory tract diseases, cardiovascular disease, etc [1, 2]. that may lead to risk of severe condition. Moreover, the disease has an impact on quality of life, especially in children [3, 4]. The caries management at the beginning mainly focuses on restoration. However, the prevalence of caries remains high. This condition may be caused by the limitation of lesion detection and also the failure of restorations. Over decades, the direction of management shifts from restoration to prevention but the disease has still high prevalence. A clinical judgment in management of caries may be one of the reasons of the remaining of the high prevalence. The caries risk assessment is introduced to solve this problem since it gives information on individual risk of caries status and also the dominant etiological factors. This information allows the physician to select the particular treatment and prevention program for a patient [5, 6].

The number of mutans streptococci (MS) is one of factors determined for the risk of caries since there are evidences showing the association between MS and caries status [7]. The culture-based method is still widely used to determine the number of MS. However, the method requires laboratory skill, equipment and also time for bacterial growth so it is impractical in clinical setting and community field. With this limitation, the chair-side commercial kits are developed. Even if it is easy to use and has efficiency similar to the conventional method, it still requires an incubator and time to grow bacteria. The rapid detection kit based on antigen and antibody reaction is developed in order to determine the number of bacteria within

15 minutes. There is a study showing that this immunodetection method has higher efficiency to evaluate the number of MS than the conventional method but the specificity (90.6%) of the method still needs to be improved. [8]

Automutanolysin (Aml) is a peptidoglycan hydrolase produced by *Streptococcus mutans*. The enzyme selectively digests mutans streptococci, *S. mutans* and *Streptococcus sobrinus*, which are human dental caries pathogens [9]. The substrate specificity towards MS is corresponded to a cell wall binding domain (CWBD) of the enzyme (unpublished observation). With this substrate specificity, CWBD can be a probe for detection of MS.

Magnetic separation in combination with size-selective membrane filtration is a method recently introduced as a versatile, simple and effective method for bacteria separation/detection [10, 11], Such method is suitable for rapid, low-cost and easy sensing of pathogen [12]. In this procedure, there are two key steps. The first step is the magnetic separation in which target pathogens in the sample are captured and isolated from the medium using the external magnet [10, 13, 14]. Magnetic nanoparticles (MNPs) are usually in magnetite form (formula is  $\text{Fe}_3\text{O}_4$ ) and have size in a range of 5 to 500 nanometers which can be attracted to magnet [15]. From aforementioned properties,  $\text{Fe}_3\text{O}_4$  have been especially useful for the rapid magnetic separation of bacteria due to response to magnetic field and their large surface to volume ratio that induces an efficient interaction with the target bacteria even in a dilute sample containing various background materials [11, 16]. After capturing and isolating the pathogens using magnetic separation, the complex collected solution is poured onto a membrane and then vacuum-filtered. Through this process, the bacteria bound MNPs are concentrated on the filter membrane. If the MNPs can bind to bacteria, the size of the pathogen bound MNPs would become much larger so that they cannot go through the pores and retained on the

membrane. Without specific binding with bacteria, the complex should remain relatively unchanged and can easily pass through the filter membrane [17, 18]. The intensity of brown spots produced by bacteria-bound MNPs on the filter membrane can be converted to numeric values of pathogen.

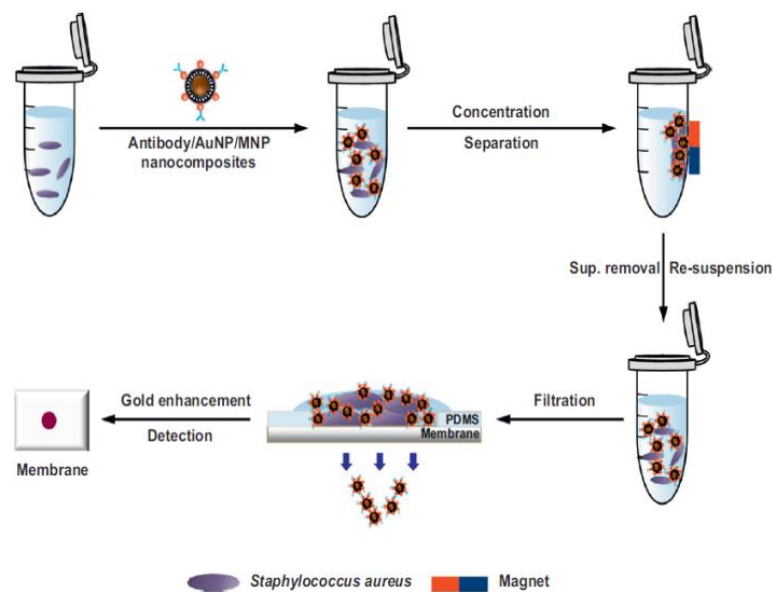
A number of research work have been reported on detection of bacteria by using MNPs nanocomposites.

In 2009, Cheng *et al.* [19] prepared the amine-functionalized magnetic nanoparticles (BMNPs) and immobilized with a specific anti-*E.coli* antibody for detection of *Escherichia coli* (*E. coli*) in pasteurized milk. The *E. coli* captured by magnetic nanocomposites so that they could be isolated easily from the sample solution by employing a permanent magnetic. The concentration of *E. coli* captured with the BMNPs was then detected by ATP bioluminescence assay. The method could detect *E. coli* in pasteurized milk ranging from  $2 \times 10^1$  to  $2 \times 10^6$  CFU/mL.

In 2009, Tunturk *et al.* [20] have reported both the activity and specific binding capacity of ferritin antibodies on the surface of MNPs. Silica-, silver- and polydopamine (PDA)-coated MNPs were first modified with 3-aminopropyltriethoxysilane (APTES) then conjugated anti-ferritin by using 1-ethyl-3-(3-dimethylaminopropyl)-carbodiimide (EDC)/ N-hydroxysuccinimide (NHS) coupling chemistry. Among all anti-ferritin-conjugated MNPs, the PDA-coated MNPs showed higher activity and stronger affinity for the specific antigen than others.

In 2013, Sung *et al.* [17] prepared novel antibody/AuNP/MNP nanocomposites for the rapid colorimetric detection of *Staphylococcus aureus* (*S. aureus*) in the pure and milk samples. MNPs and AuNPs were used as platforms for magnetic separation and signal generation, respectively. The nanocomposites were synthesized by coating the MNPs with bovine serum albumin (BSA). The AuNPs were effectively attached to

the MNPs surface by electrostatic interactions with BSA. After that, anti-*S. aureus* was conjugated with nanocomposites via EDC/NHS coupling. The overall concept of bacterial detection is displayed in Figure 1.1. The target bacteria in the pure sample could be detected with LOD of  $1.5 \times 10^3$  CFU/mL while  $1.5 \times 10^5$  CFU/mL of *S. aureus* in the milk sample could be distinguished from the negative control.

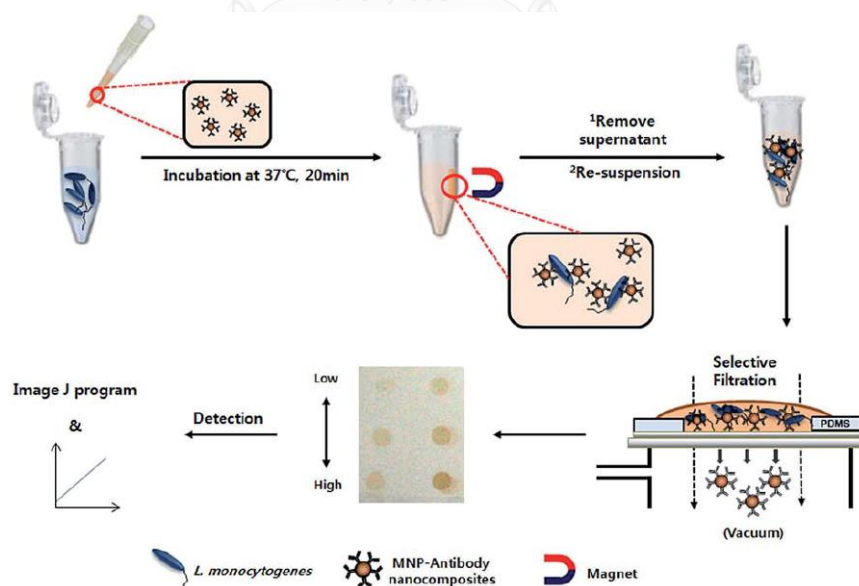


**Figure 1.1** Magnetic separation and colorimetric detection process for the *S. aureus* sensing using antibody/AuNP/MNPs and selective filtration method.

In 2014, Shim *et al.* [18] developed a selective filtration method using MNPs modified with monoclonal antibody (MAb) for the rapid and sensitive colorimetric detection of *Salmonella typhimurium* (*S. typhimurium*). Antibody was immobilized on MNPs using EDC as a coupling agent. The MAb-MNPs nanocomposites were isolated using a magnet. After that, the nanocomposites were transferred onto the filter membrane with 0.8 micron pore size under vacuum. The color intensity on the membrane was quantified and averaged for each sample. The detection limit (LOD) of the method was found to be  $1.5 \times 10^3$  CFU/mL.



In 2014, Shim *et al.* [12] developed the method for the rapid colorimetric detection of *Listeria monocytogenes* (*L. monocytogenes*) by using MNPs nanocomposites. The MNPs were conjugated with monoclonal antibody (MAb) which is specific to *L. monocytogenes* via EDC/NHS coupling. The nanocomposites bound and unbound to *L. monocytogenes* after being isolated by an external magnet were directly passed through the polydimethylsiloxane (PDMS) membrane by vacuum filtration, and the color signals from bacteria-MNPs nanocomposites that remain on the membrane were measured, reflecting the amount of *L. monocytogenes* in a sample. The concept is shown in Figure 1.2. The method could detect *L. monocytogenes* in the samples in a concentration range of  $2 \times 10^1$  to  $2 \times 10^3$  CFU/mL. Capture efficiencies of the MNPs nanocomposites were confirmed to be 48, 63 and 89% for bacteria having concentration of  $10^3$ ,  $10^2$ , and  $10^1$  CFU/mL, respectively. The limit of detection (LOD) of the method in a pure pathogen solution and vegetable samples were  $2 \times 10^3$  and  $1 \times 10^2$  CFU/mL, respectively.



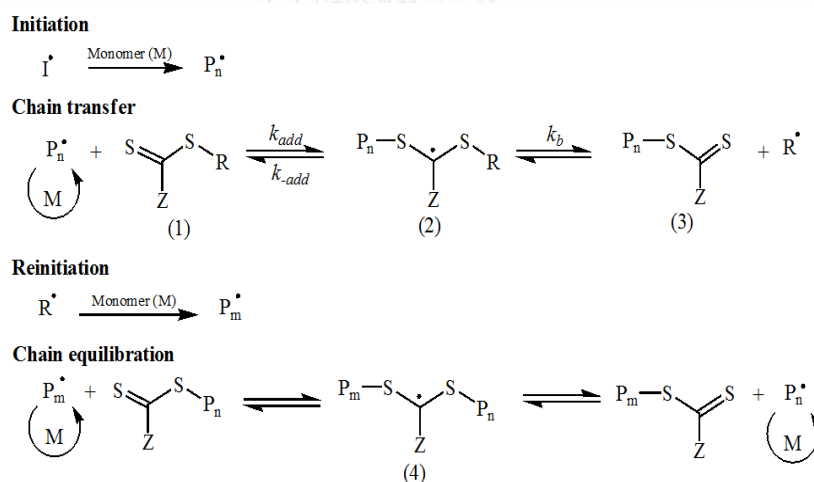
**Figure 1.2** Schematic diagram of a selective filtration method based on a monoclonal antibody (MAb)-conjugated magnetic nanoparticle (MNP) for the rapid and sensitive detection of *L. monocytogenes* [12].

Although a number of researches have been reported on the detection of bacteria, all of them are based on antibody-conjugated with MNPs, To the best of our knowledge, there have been no reports on the use domain of enzyme generated by bacteria as biomolecular probe for the assay based on magnetic separation/selective filtration and none have been reported on the detection of mutans streptococci for caries risk assessment.

A number of polymers such as dextran, [21] polystyrene (PS), [22, 23] poly(acrylic acid) (PAA) [24, 25] have been coated on MNPs to increase stability and dispersibility of the MNPs. The polymeric stabilizer can increase the affinity of MNPs for specific solvent and inhibit particle aggregation [26-29]. Polymer-grafted MNPs nanocomposites formed a very stable dispersion in organic solutions and remained dispersed for an extended period of time [30-32]. Among the methods for preparing polymer-coated nanoparticles, surface functionalization by grafting of polymer is one of the most effective methods. The surface properties can be widely changed by choosing a variety of functional monomers. Two methods are generally used to functionalize nanoparticles via the formation of covalent polymer-bounded layers onto the surface of particles: “grafting from” and “grafting onto” [33]. The “grafting from” method involves polymer chain growing from surface-attached initiator. So, this method provides high grafting density. For the “grafting to” method, polymer is grafted on the surface. The method is simple, but the grafting density may be low because steric hindrance of the polymer chains previously attached to the surface. MNPs can be functionalized well-defined polymers of desired grafting density using either method. Recently, surface-initiated graft polymerization to control the molecular weight of the graft chains on MNPs using several techniques such as free radical polymerization cationic and anionic [30, 33-35]. The polymerization that yield

polymer well-controlled molecular weight and molecular weight distribution of polymer chain can be called controlled polymerization [26, 36, 37]. RAFT polymerization is one of a controlled radical polymerization method that has widely been applied for polymerization of a wide range of functional monomers such as acrylic acid, [38] styrene, [22] (meth)acrylates [30].

The RAFT process is a controlled radical polymerization technique that operates via a degenerative transfer mechanism in which a thiocarbonylthio compound acts as a chain transfer agent (Figure 1.3). RAFT polymerization provides many advantages: applicability for various water-soluble monomers, lack of metal catalyst use which is desirable for using in bio-application.



**Figure 1.3** Generally accepted mechanism for RAFT polymerization.

Many research works have reported on preparation of polymer-grafted MNPs nanoparticles via RAFT polymerization:

In 2006, Wang, *et al.* [22] synthesized MNPs nanoparticles grafted with polystyrene (PS) and poly(acrylic acid) (PAA) via RAFT process. Peroxides and hydroperoxides were generated on the surface of MNPs nanoparticles via ozone

pretreatment. Ozone pretreatment was similarly used to introduce active species on the surface of the MNPs, which then acted as macroinitiators for polymerization of styrene and acrylic acid. Under thermal induction, the peroxide functional groups undergo decomposition to initiate the free radical graft polymerization of vinyl monomers. The resulting core-shell MNPs-g-PS and MNPs-g-PAA nanocomposites formed stable dispersions in the organic solvents for PS and PAA, respectively.

In 2008, Chiu *et al.* [39] have reported the immobilization of PAA (MW ~ 2 kDa) onto the surface of magnetic nanoparticles. PAA contains a number of active carboxyl groups which are capable of chelating with Fe<sub>3</sub>O<sub>4</sub> nanoparticles and acting as proton source for protonation of analyte. The PAA-grafted MNPs nanocomposites can be used as matrix for surface-assisted laser desorption ionization-mass spectrometry (SALDI-MS) analysis without the addition of extra proton source. Biomolecules, namely bradykinin, mellitin, and insulin were used as samples for feasibility test. The upper detectable mass limit in this report was ~6 kDa.

In 2011, Wang, *et al.* [40] grafted diblock copolymer brushes of poly(ethylene glycol) monomethacrylate and N-isopropylacrylamide (P(PEGMA)-*b*-PNIPAA) on the surfaces of magnetic nanoparticles (MNPs) using surface-induced RAFT polymerization with the aim to decrease the non-specific adsorption of proteins on MNPs. The diblock copolymer brushes on MNPs surfaces were synthesized MNPs modified with P(PEGMA)-*b*-PNIPAA was incubated with bovine serum albumin (BSA), lysozyme and  $\gamma$ -globulin. The UV-vis absorbances of proteins incubated with P(PEGMA)-*b*-PNIPAA-MNPs rarely decreased suggesting that no proteins were adsorbed on the modified MNPs. From the results, the grafted P(PEGMA)-*b*-PNIPAA can decrease the nonspecific adsorption of protein on MNPs.

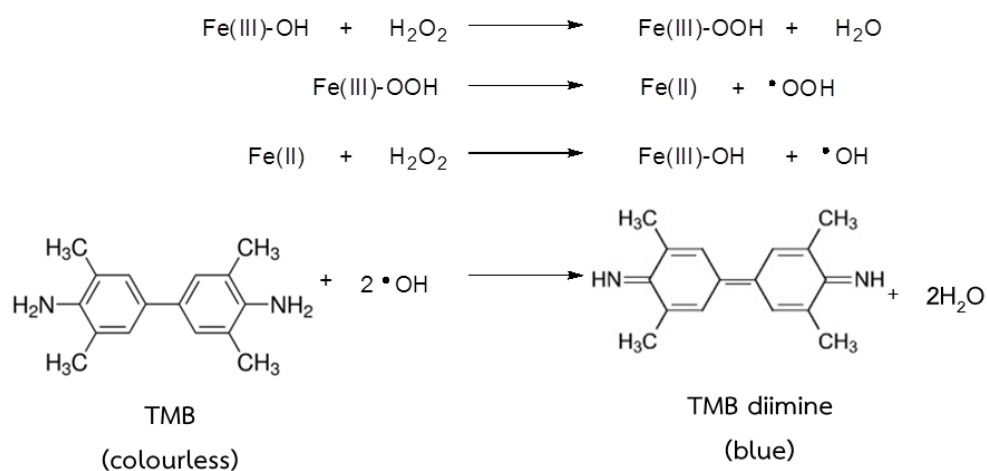
In 2013, Sahoo *et al.* [37] prepared magnetite nanoparticles (MNPs) grafted with poly(*N*-isopropylacrylamide)-*block*-poly(acrylic acid) (PNIPAM-*b*-PAA) copolymer for targeted delivery of anticancer drug. PNIPAM-*b*-PAA was synthesized by RAFT polymerization and then attached to the amine-functionalized MNPs via EDC/NHS method. After that, doxorubicin (DOX), an anticancer drug was loaded into the nanocomposites. From *in vitro* investigation, DOX-loaded nanocomposites achieved excellent efficacy for simultaneously targeting and destroying cancer cells. DOX-MNPs nanocomposites release the anticancer drug preferably at pH 5.0 and temperature of 37 °C.

In 2015, Li, *et al.* [26] prepared superparamagnetic iron oxide nanoparticles (SPIONs) loaded with polymeric micelles by self-assembly of amphiphilic (poly(2,2,3,4,4,4-hexafluorobutyl methacrylate-*co*-methacryloxyethyl trimethyl ammonium chloride)-*g*-poly(ethylene glycol) monomethacrylate) copolymers which was synthesized via RAFT polymerization and conjugated with folate bovine serum albumin (FA-BSA) specific tumor marker by electrostatic interactions. FA-BSA modified and SPIONs-loaded polymeric micelles were used for studying folate-receptor overexpressed cancer targeting and MR imaging *in vitro* and *in vivo*. From experiment, magnetic micelles can be specifically assembled into the tumor tissues *in vivo*. It was also found that a limited contribution of passive mechanisms to tumor tissue retention of the magnetic micelles.

In 2016, Dutta, *et al.* [38] synthesized poly(*N*-isopropylacrylamide-*ran*-poly(ethylene glycol) methyl ether acrylate)-*block*-poly(acrylic acid) (P(NIPAM-*r*-PEGMEA)-*b*-PAA) synthesized by RAFT polymerization was covalently grafted on APTES-modified iron oxide surfaces. *In vitro* controlled release of DOX from the nanocomposites in different pH and temperature were investigated. As evaluated by MTT assay, apoptosis of ME 180 cervical cancer cells were found in the presence of

the polymer-iron oxide nanocomposites loaded with DOX suggesting that DOX can be released desired at lysosomal pH (pH=5) and temperature (T=37 °C) within cancer cells.

MNPs have the properties of magnetic separation and enrichment.  $\text{Fe}_3\text{O}_4$  possess intrinsic peroxidase-like activity, which can catalyze oxidation of 3,3',5,5'-tetramethylbenzidine (TMB) and hydrogen peroxide ( $\text{H}_2\text{O}_2$ ) to develop colour reaction [41, 42]. MNPs exhibited an intrinsic enzyme mimetic activity similar to that found in HRP (horseradish peroxidase) and natural peroxidase, though MNPs nanocomposites are usually thought to be biological and chemical inert [43]. MNPs enzyme mimics have several advantages above traditional natural enzymes, (a) the catalytic property of MNPs nanocomposites is more stable than the peroxidases such as HRP, which is weak to the reaction conditions. (b) iron oxide nanocomposites have the properties of magnetic separation and enrichment, which can facilitate the biological applications. (c) The preparation of MNPs is basic and low cost, while the preparation and purification of natural enzymes are usually time-consuming and expensive. (d) MNPs nanocomposites are able to catalyze the color reaction in a much broader pH range than standard enzymes and (e)  $\text{Fe}_3\text{O}_4$  nanocomposites can be used to capture and separate the pathogen from the sample with a permanent magnet, which integrates the sample preparation with demonstration, thus, accommodates the all analysis process [44, 45].



**Figure 1.4** TMB can act as a hydrogen donor for the reduction of hydrogen peroxide to water by MNPs nanocomposites, the resulting diimine causes the solution to take on a blue color.

Many research works has been reported on the use of MNPs nanocomposites to catalyze the color reaction of TMB in the presence of  $\text{H}_2\text{O}_2$ :

In 2008, Zhuang, *et al* [45] develop a spectrometric method using MNPs as catalyst to measure  $\text{H}_2\text{O}_2$  in rainwater. In this experiment, MNPs and HRP were used to catalyze the oxidative reaction of  $\text{H}_2\text{O}_2$  to develop color reaction and the limit of detection (LOD) was investigated. From the results, the limit of detection (LOD) for MNPs and HRP in  $\text{H}_2\text{O}_2$  sample was found to be  $1.75 \times 10^{-7}$  and  $1 \times 10^{-7}$ , respectively. This data suggested that MNPs could be used as a promising catalyst, which possess equivalent detection limit as compared with HRP.

In 2008, Gao, *et al* [41] developed a magnetic nanoparticle-linked immunoassay by using chitosan-modified iron oxide nanoparticles (CS-MNPs) as a replacement of enzymes in conventional ELISA configuration. The color reaction of TMB in the presence of  $\text{H}_2\text{O}_2$  was used to demonstrate the catalytic activity of the CS-MNPs. Chitosan was employed to prevent aggregation and promoted dispersion of

MNPs in aqueous solutions. CS-MNPs were functionalized with anti-CEA (Carcinoembryonic antigen) antibody (M111147) through cross-linking amine groups on the surface of the MNPs with the amine groups of the antibodies via glutaraldehyde. The functionalized MNPs were mixed with the samples containing CEA in different concentrations. The number of CEA in the sample was quantified by measuring the optical density at 652 nm. From a result of the assay, this capture-detection immunosorbent assay based on CS-MNPs has a detection limit of about 1 ng/ml for CEA.

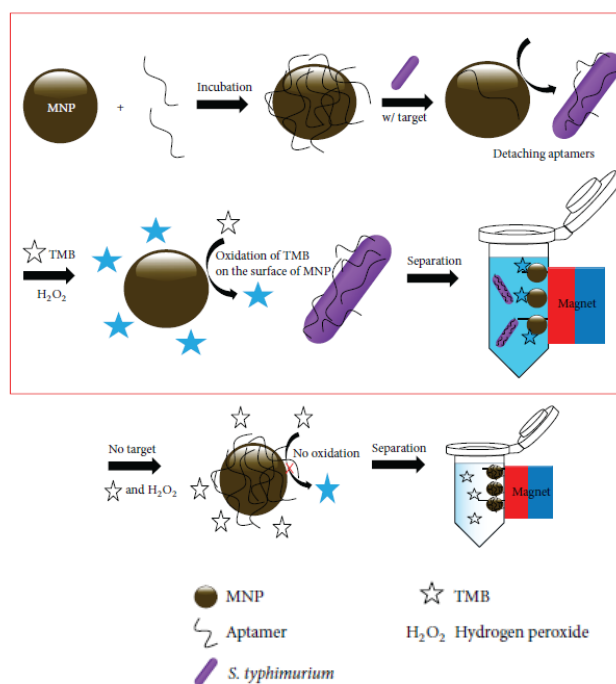
In 2010, Zhang, *et al* [43] developed MNPs-linked colorimetric assay for the determination of thrombin based on the enzyme-linked immunosorbent assay (ELISA). Chitosan-modified iron oxide nanoparticles (CS-MNPs) were synthesized and used as peroxidase mimic for the determination of thrombin. Biotinylated thrombin aptamer 1 was first loaded into a 96-well plate by streptavidin binding. Then, amino-terminal thrombin aptamer 2 was conjugated to the CS-MNPs via glutaraldehyde coupling. After that, a sample and aptamer 2 conjugated MNPs were added into the 96-well plate having immobilized aptamer 1. The signal due to the binding was then amplified by having MNPs acting as peroxidase catalyst for TMB in the presence of  $H_2O_2$ . The results showed that the calibration curve of absorption values at 652 nm with the thrombin concentrations was linear in a range from 1 to 100 nM and the limit of detection (LOD) was estimated to be 1 nM.

In 2013, Woo, *et al* [42] detects retroviruses and breast cancer cells by using MNPs nanocomposites. Magnetic nanoparticle (MNPs) was immobilized with monoclonal antibody (MAb), which is specific to retroviruses or breast cancer cells. After the MAb-functionalized MNPs were bound with the target microorganism, TMB and  $H_2O_2$  were added to the sample to produce detection signals, which reflected the amount of retroviruses and breast cancer cells in the sample. The catalytic



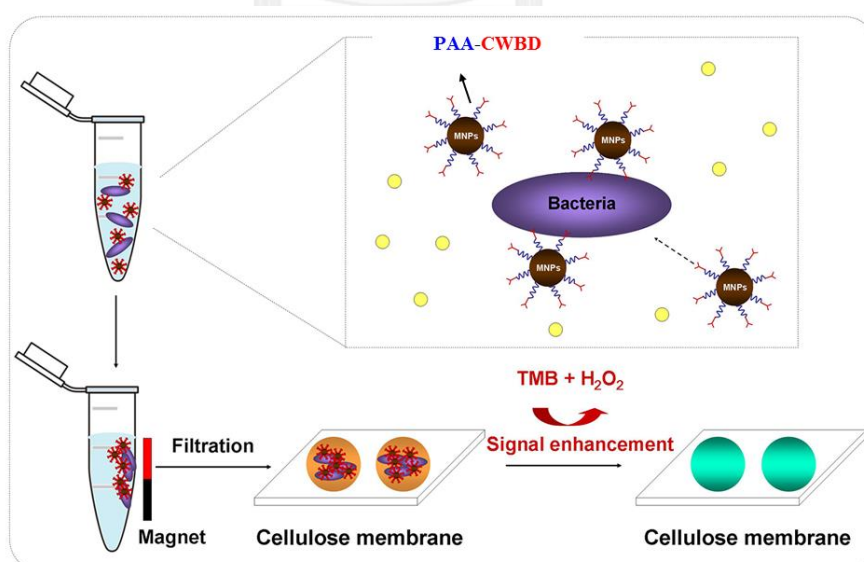
activity of HRP and MNPs-MAb were compared. It was found that the catalytic activity of MNPs is more stable than HRP.

In 2015, Park *et al.* [44] developed a rapid colorimetric system based on MNPs and DNA aptamers for the detection of *Salmonella typhimurium* (*S. typhimurium*), which relies on increasing signal from the peroxidase-like activities of MNPs (Figure 1.5). MNPs display enzyme-like activities, they can undergo color changes with the help of a colorimetric substrate. MNPs were first incubated with aptamers that specifically interact with the *Salmonella* species. After the addition of *S. typhimurium* to the solution, specific aptamers on the MNPs interact with the *Salmonella*. Bacteria bound MNPs nanocomposites were concentrated by a magnet, followed by signal enhancement by the peroxidase activity of the MNPs. From the intensity of absorbance at 650 nm, the aptamers-MNPs nanocomposites can be used for the colorimetric detection of *S. typhimurium*.



**Figure 1.5** Schematic illustration of the MNP-based colorimetric detection using label-free DNA aptamers and TMB [44].

Inspired by aforementioned research, this research aims to develop a versatile, simple and effective method for mutans streptococci separation/detection based on magnetic separation in combination with size-selective filtration method using CWBD-conjugated magnetic nanoparticles (CWBD-conjugated MNPs) following the concept shown in Figure 1.6. MNPs were first grafted with poly(acrylic acid) (PAA) via RAFT polymerization. The CWBD was then conjugated with carboxyl groups of PAA via EDC/NHS coupling chemistry. The assay consists of two key steps. First, external magnetic field was applied to separate and concentrate *S. mutans* along with CWBD-conjugated MNPs from tested solution. The *S. mutans*-bound CWBD-conjugated MNPs isolated by external magnet are then filtered through a nitrocellulose membrane by vacuum. With appropriate pore size of the membrane, the *S. mutans*-bound CWBD-conjugated MNPs remained on the membrane can be detected colorimetrically by naked eye. Taking advantage of peroxidase-like activity of MNPs, the signal was further amplified by introducing TMB as a substrate together with  $H_2O_2$  on membrane surface.



**Figure 1.6** Schematic representation of colorimetric detection of mutans streptococci with MNPs grafted with PAA and immobilized with CWBD of Automutanolysin.

## 1.2 Objectives

1. To prepare and characterize the CWBD-conjugated MNPs
2. To study the usage of the CWBD-conjugated MNPs for detection of mutans streptococci.

## 1.3 Scope of investigation

The stepwise investigation was carried out as follows:

1. Literature survey for related research work.
2. To synthesize and characterize MNPs by solvothermal method.
3. Preparation and characterization of PAA-grafted MNPs by surface-initiated RAFT polymerization.
4. Immobilization of CWBD of Automutanolysin on PAA-grafted MNPs via EDC/NHS coupling.
5. Separation and colorimetric detection of mutans streptococci using CWBD-conjugated MNPs by magnetic separation and selective filtration method.

## CHAPTER II

### EXPERIMENTAL

#### 2.1 Materials

Iron (III) chloride hexahydrate ( $\text{FeCl}_3 \cdot 6\text{H}_2\text{O}$ ) was purchased from Merck. 3-Aminopropyltriethoxysilane (APTES), 4,4-azobis(4-cyanovaleric acid) (ACVA), 4-cyano-4-(phenylcarbonothio) pentanoic acid (CPD), 4-(dimethylamino)pyridine (DMAP), *N,N'*-dicyclohexylcarbodiimide (DCC), dimethylformamide (DMF), urea-hydrogen peroxide ( $\text{H}_2\text{O}_2$ ) and 3,3',5,5'-tetramethylbenzidine (TMB), 1-ethyl-3-(3-dimethylaminopropyl)-carbodiimide (EDC), *N*-hydroxysuccinimide (NHS), acrylic acid monomer (AA), sodium acetate (NaAc) and ethylene glycol were bought from Sigma-Aldrich. Phosphate buffered saline (PBS, pH 7.4), and cellulose acetate membrane (CA membrane) with a 0.2, 0.45, 0.8 and 1.2  $\mu\text{m}$  pore size were purchased from Chemical Express. All reagents and materials are analytical grade and used without further purification. Ultrapure distilled water was obtained after purification using a Millipore Milli-Q system (USA) that involves reverse osmosis, ion exchange and a filtration step.

#### 2.2 Equipments

##### 2.2.1 Fourier Transform-Infrared Spectroscopy (FT-IR)

The FT-IR spectra were recorded in KBr discs with a FT-IR spectrometer (Nicolet, USA), model Impact 410, with 32 scans at resolution  $4\text{ cm}^{-1}$ . A frequency of  $400\text{-}4000\text{ cm}^{-1}$  was collected by using TGS detector.

##### 2.2.2 Thermogravimetric Analysis (TGA)

Thermogravimetric analysis (TGA) was carried out employing a Diamond TG/DTA (PerkinElmer Instruments, China) and tests were operated under a

dynamic nitrogen atmosphere flowing in a temperature range of 30-900°C and the heating rate was set at 20°C/min.

### **2.2.3 Transmission Electron Microscopy (TEM)**

The morphology and actual size of particles were evaluated by a JEOL JEM-2010 transmission electron microscopy (TEM) (Japan) operated at 120 kV equipped with Gatan model 782 CCD camera. A sample solution in Milli-Q water was directly cast onto carbon-coated copper grids and dried in a desiccator prior to analysis. The average diameters were reported from measurements of 30 random particles for each sample using Semafore software.

### **2.2.4 X-ray Diffraction (XRD)**

The phase structures of MNPs were characterized by powder X-ray diffraction (XRD, D/Max) with CuK $\alpha$  radiation ( $\lambda$  radiation = 0.15418 nm).

### **2.2.5 Dynamic Light Scattering (DLS)**

The particle size and zeta potential of the MNPs were measured by dynamic light scattering (DLS). The MNPs suspensions were diluted in Milli-Q water and placed into a cuvette. The measurements were taken at 25°C three times for each sample using Malvern Nano ZS90 Instruments Ltd., Worcestershire, UK to determine the intensity average size distribution and z-average diameter. Zeta-potential measurements of these MNPs suspensions were also determined using the same instrument. The suspensions were diluted with Milli-Q water and added into zeta-cell and measurements were taken three times for each sample at 25°C.

### **2.2.6 Scanner**

The scanned images of the tested results on filter papers were recorded on Epson Perfection V33 scanner in 24 bits Professional mode. The brightness/contrast/resolution was set to 128/128/300. The images were saved as

TIFF-files. The intensity of each spot was determined using Scion Image software by first converting to gray scale at 300 dpi. Intensity measurements were carried out using the Line tool to select area for analysis to obtain profile images.

## 2.3 Experimental Procedure

### 2.3.1 Preparation of Cell Wall Binding Domain of Automutanolysin

The cell wall binding domain (CWBD) gene was amplified by polymerase chain reaction (PCR) using *Streptococcus mutans* genome as a template. The amplified gene was inserted into pColdIII that was modified to carry histidine nucleotide sequences. The recombinant plasmid was then transformed into *Escherichia coli* BL-21. To express the His-tagged CWBD protein, *E. coli* BL-21 was grown until reach  $OD_{600nm}$  of 0.4-0.6 and then induced the expression of protein by an addition of 1 mM isopropyl- $\beta$ -D-thiogalactoside (IPTG) and incubated at 15°C for 24 h. The protein was purified using HIS-Select<sup>®</sup> Nickel Affinity Gel (Sigma-Aldrich Corp., St. Louis, MO, USA) under native condition. The active fractions will be pooled and dialyzed against 0.1 M phosphate buffer (pH 6.8). The concentration of protein was measured by using the Bradford protein assay.

### 2.3.2 Synthesis of MNPs by Solvothermal Method

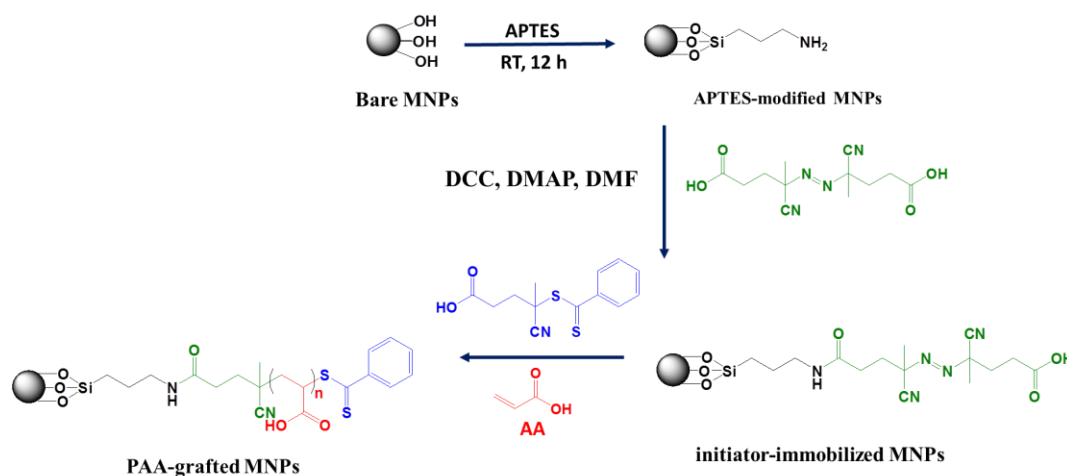
In a typical procedure for the preparation of MNPs by solvothermal method, 1.35 g  $FeCl_3 \cdot 6H_2O$  was dissolved in 20 mL of ethylene glycol with vigorous stirring. After the solution became colorless, 3.6 g NaAc was added with continuous stirring for 30 min at room temperature. Then the mixture was transferred into a 50 mL Teflon-lined stainless-steel autoclave and reacted at 170 °C for 12 h. After the reaction was complete, the autoclave was cooled down to room temperature. The formed black  $Fe_3O_4$  nanoparticles were collected under external magnetic field,

rinsed with ethanol for 10 times, and dried at 60 °C to yield black powder of MNPs. (69% yield)

### 2.3.3 Preparation of PAA-grafted MNPs

PAA was grafted on MNPs surface via “grafting from” method. MNPs were first immobilized with APTES. Briefly, 0.1 g of MNPs was first dispersed ultrasonically in 100 mL of 9:1 (v/v) ethanol-water mixture having added 1 mL of ammonia solution for 30 min. To the above dispersed solution, 1 mL of APTES was added dropwise and the resulting mixture was stirred at room temperature for 12 h. Thereafter, the obtained APTES-modified MNPs were magnetically concentrated, washed thoroughly with ethanol, and then was vacuum dried.

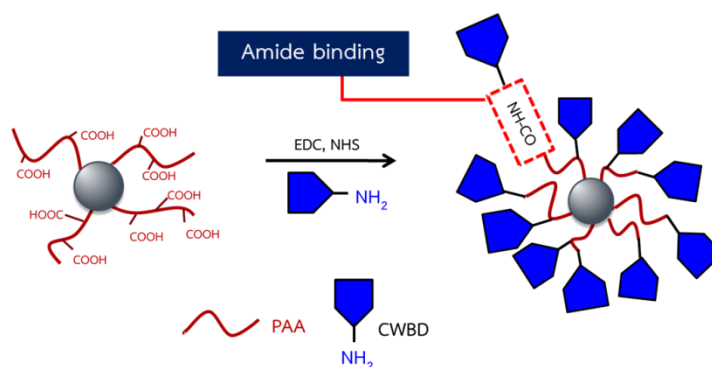
The APTES-modified MNPs were immersed in 20 mL DMF containing ACVA (37.5 mmol), DCC (47.0 mmol) and DMAP (3.74 mmol) at room temperature for 20 h under nitrogen atmosphere. After the reaction was complete, the product was rinsed thoroughly with DMF and ethanol for four times each. The obtained initiator-immobilized MNPs were then placed in a vial containing ACVA (0.5 mmol), CTA (5 mmol), and AA (0.8 mol) in 10 mL of Milli-Q water. The vial was then placed in a pre-heated oil bath at 70 °C for 20 h under nitrogen atmosphere. The resulting surface-grafted PAA were removed from the vial and washed with ethanol and Milli-Q water, respectively (Figure 2.1).



**Figure 2.1** Preparation of PAA-grafted MNPs via surface-initiated RAFT polymerization

### 2.3.4 Immobilization of CWBD on PAA-grafted MNPs

PAA-grafted MNPs were conjugated with CWBD of Automutanolysin via the EDC/NHS coupling method as follows. 5 mg of PAA-grafted MNPs were dispersed in 1 mL of 0.01 M PBS, pH 7.4. To this, 0.1 mL of EDC (2 M) and NHS (0.5 M) were added to and then the mixture was incubated for 30 min at room temperature under shaking at 240 rpm on a rotary shaker. 0.1 mL of CWBD (1 mg/mL) was added to the mixture and incubated for 24 h at 4 °C. Finally, the CWBD-conjugated MNPs were isolated using a magnet and rinsed with 0.01 M PBS, pH 7.4 and milli-Q water, respectively. The product was stored at 4 °C until use.



**Figure 2.2** Conjugation of CWBD with PAA-grafted MNPs via EDC/NHS coupling.



### 2.3.5 Oxidative Catalytic Property of MNPs.

In a typical procedure, TMB solution (10 mg/mL in DMSO) and H<sub>2</sub>O<sub>2</sub> (30 % (w/w) in H<sub>2</sub>O) were consecutively spotted on a membrane. After 50 s, the membrane was washed with Milli-Q water. The color intensity of the membrane was quantified and averaged from three independent samples for each sample using the scanned images of the tested results on the filter membrane recorded on Epson Perfection V33 scanner in 24 bits Professional mode. The quantity of each reagent was varied to find an optimal ratio for signal amplification as shown in Table 2.1

**Table 2.1** Various quantities of TMB, H<sub>2</sub>O<sub>2</sub> and MNPs for optimization.

Reagent	Quantity
TMB (10 mg/mL in DMSO)	0, 0.5, 1, 1.5, 2, 2.5 and 3 $\mu$ L
H <sub>2</sub> O <sub>2</sub> (30 % (w/w) in H <sub>2</sub> O)	0, 0.1, 0.2, 0.3, 0.4, 0.5, 0.6, 0.7, 0.8, 0.9, 1.0 and 1.1 $\mu$ L
MNPs	0, 0.05, 0.1, 0.15, 0.2, 0.25, 0.3, 0.35, 0.4, 0.45 and 0.5 mg

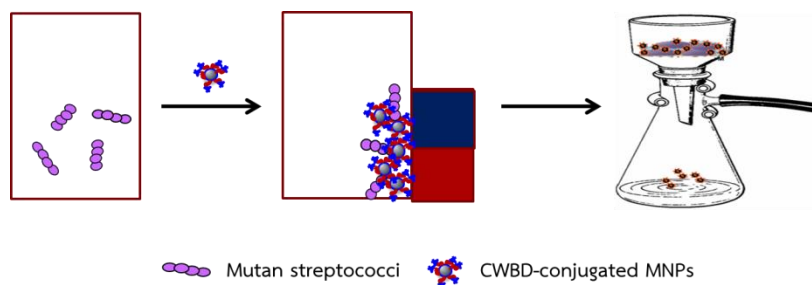
### 2.3.6 Bacterial Culturing

*S. mutans*, *S. sobrinus*, *S. salivarius* and *S. sanguinis* were cultured in brain heart infusion (BHI) broth at 37 °C under 5% CO<sub>2</sub> atmosphere with 180 rpm shaking for 24 h. The optical density of 24-hours culture was measured at the wavelength 600 nm. The cultures were then diluted to OD<sub>600nm</sub> of 0.1 and incubated for 2.5 h to obtain OD<sub>600nm</sub> of 0.5 ( $\approx 10^{10}$  CFU/ml). After that, the bacterial cultures

were ten-fold serially diluted from  $10^7$  to  $10^2$  CFU/ml with 0.01 M PBS, pH 7.4. The colony count was performed to verify the number of bacteria.

### 2.3.7 Determination of Bacteria Capturing by CWBD-conjugated MNPs

Capturing of designated bacterial strain (*S. mutans*, *S. sobrinus*, *S. salivarius* and *S. sanguinis*) by CWBD-conjugated MNPs was determined. Briefly, 0.1 mL of bacterial solution having varied concentration in a range of  $1 \times 10^2$  to  $1 \times 10^7$  CFU/mL was transferred into 1.5 mL tube containing 0.2 mL of CWBD-conjugated MNPs solution (0.15 mg/mL in 0.01 M PBS, pH 7.4) and then incubated for 30 min at 4 °C. After incubation, the tube was placed in a magnet for 10 min to isolate and concentrate the bacteria-bound CWBD-conjugated MNPs. The supernatant was removed and bacteria-bound CWBD-conjugated MNPs were re-suspended in 0.1 mL of 0.01 M PBS, pH 7.4. A filter membrane with selected pore size (0.2, 0.45, 0.8, and 1.2  $\mu\text{m}$ ) was wet with 0.01 M PBS, pH 7.4 before being placed on a 1L-Erlenmeyer flask equipped with an aspirator. 50  $\mu\text{L}$  of the bacteria-bound CWBD-conjugated MNPs suspension was poured onto the membrane under vacuum, as shown in Figure 2.3. The color intensity on the membrane which reflected the amount of bacteria of the sample was quantified and averaged from three independent samples using the scanned images of the tested results on the filter membrane recorded on Epson Perfection V33 scanner in 24 bits Professional mode. For signal amplification, the membrane was consecutively spotted with optimized quantity of TMB and  $\text{H}_2\text{O}_2$  that yielded the highest signal amplification identified in 2.3.5. After 50 s, the membrane was washed with Milli-Q water. The color intensity on the membrane was quantified by a similar method as mentioned above.



**Figure 2.3** Magnetic separation and selective filtration process of mutans streptococci using CWBD-conjugated MNPs.

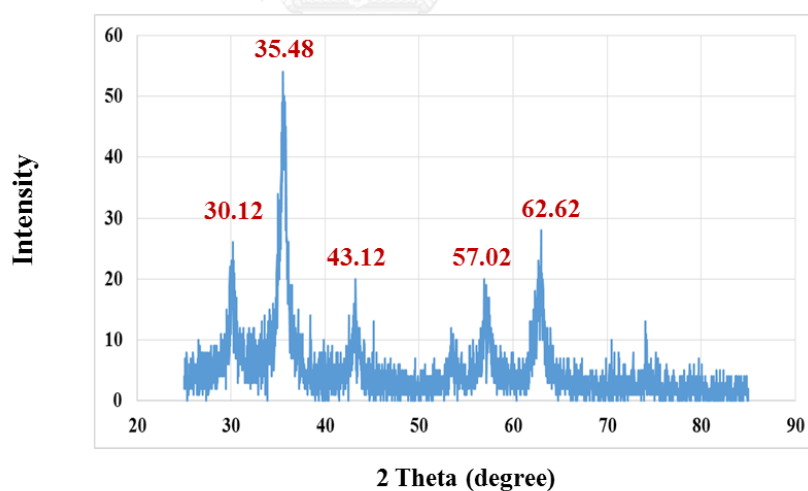


## CHAPTER III

### RESULTS AND DISCUSSION

#### 3.1 Preparation and characterization of PAA-grafted MNPs and CWBD-conjugated MNPs

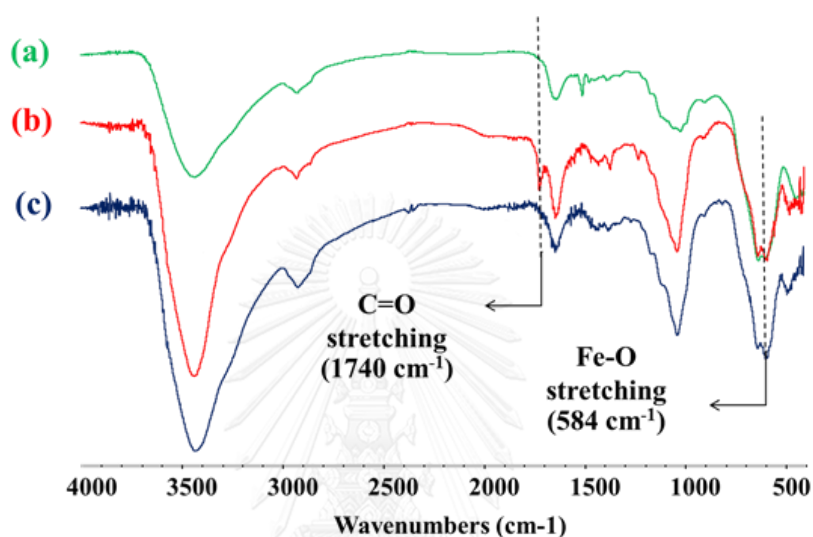
MNPs were synthesized by solvothermal method. As shown in Figure 3.1, XRD pattern of MNPs shows diffraction peaks at  $2\theta = 30.12, 35.48, 43.12, 57.02$  and  $62.62$  which can be assigned to (311), (440), (220), (511), and (400) planes of  $\text{Fe}_3\text{O}_4$ , respectively. This characteristic coincides with that of the standard magnetite (JCPDS 19-629). No other diffraction peaks corresponding to ferrite nitrite or other iron oxide, such as  $\alpha\text{-Fe}_2\text{O}_3$  and  $\gamma\text{-Fe}_2\text{O}_3$ , could be detected suggesting that the obtained MNPs are in the form of pure  $\text{Fe}_3\text{O}_4$ .



**Figure 3.1** XRD pattern of bare MNPs nanoparticles prepared by solvothermal method.

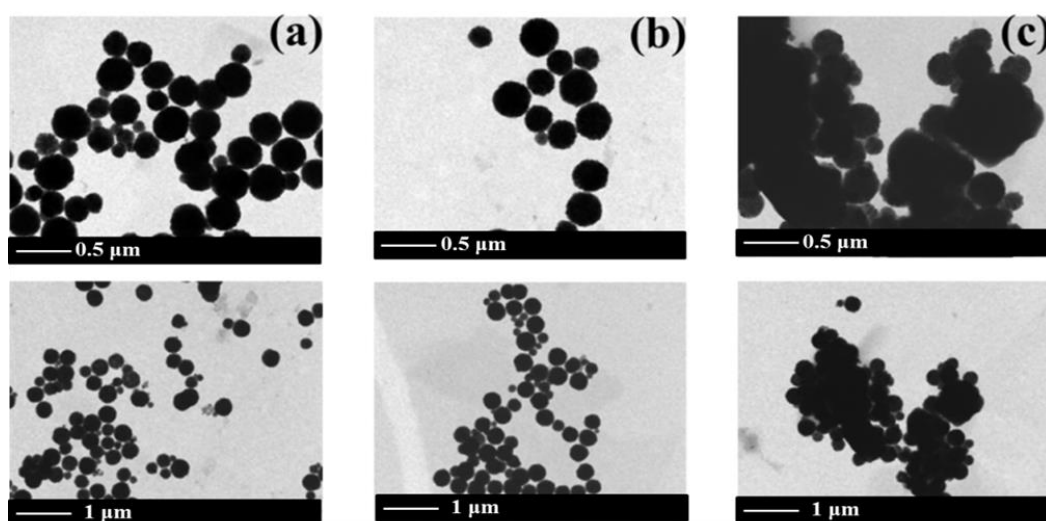
PAA-grafted MNPs was prepared by surface-initiated RAFT polymerization. The success of stepwise surface modification of MNPs was confirmed by FT-IR as shown in

Figure 3.2. A characteristic Fe-O vibration of the unmodified MNPs (Figure 3.2a) is observed at  $584\text{ cm}^{-1}$ . The spectrum of PAA-grafted MNPs (Figure 3.2b) shows a band at  $1740\text{ cm}^{-1}$ , which is assignable to C=O stretching of carboxyl groups of PAA. Such signal disappeared upon CWBD conjugation (Figure 3.2c) indicating that amide linkage was formed between carboxyl groups of PAA and amino groups of the enzyme.



**Figure 3.2** FT-IR spectra of MNPs: (a) unmodified, (b) grafted with PAA and (c) conjugated with CWBD.

Figure 3.3 illustrates the morphology of MNPs before and after modification as examined by TEM. The unmodified MNPs (Figure 3.3a) are spherical with an average diameter of  $328.2 \pm 22.7\text{ nm}$ . The average diameter of MNPs correspondingly increased upon surface modification especially after CWBD conjugation to  $357.4 \pm 19.2$  and  $745.5 \pm 29.9\text{ nm}$  for PAA-grafted MNPs (Figure 3.3b) and CWBD-PAA-MNPs (Figure 3.3c), respectively. Higher degree of aggregation was also realized in the case of CWBD-conjugated MNPs. This may be ascribable to the conjugation with relatively large molecules of CWBD (MW = 80 kDa).



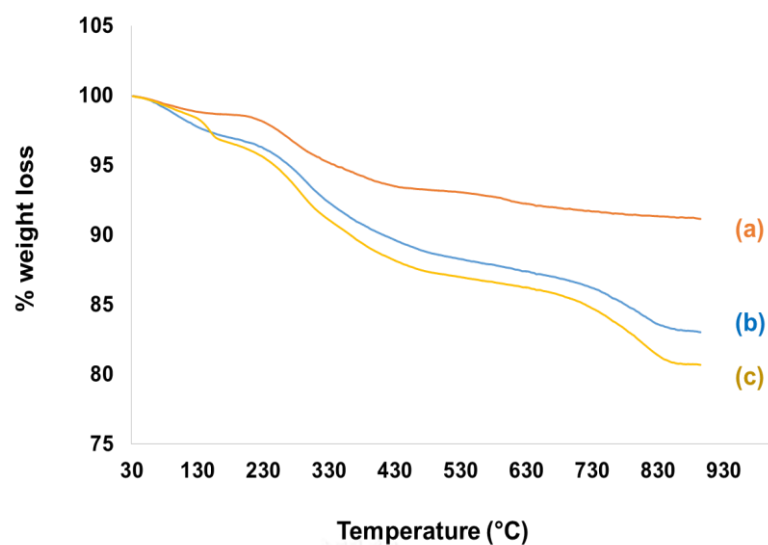
**Figure 3.3** TEM micrographs of (a) bare MNPs, (b) PAA-grafted MNPs, and (c) CWBD-conjugated MNPs (scale bar 1  $\mu\text{m}$  (top) and 0.5  $\mu\text{m}$  (bottom), respectively).

The particle size and zeta potential of the MNPs were also evaluated by DLS of which data are listed in Table 3.1. In good agreement with the TEM data, the average size of MNPs became increasingly larger after PAA grafting and CWBD conjugation. The  $\text{pK}_a$  of PAA is 4.5 [22] and the isoelectric point of CWBD [9] is approximately 5.17 which should result in both PAA and CWBD being negatively charged in PBS solution (pH of 7.4, with PAA being more negatively charged). For this reason, the PAA-grafted MNPs exhibited a negative zeta potential of -31.43 mV verifying the presence of ionizable carboxyl groups of PAA surrounding the MNPs. After CWBD conjugation, the zeta potential of the MNPs became less negative (-14.40 mV), which was due to CWBD being less negatively charged than PAA. This result indicated the successful immobilization of CWBD on the PAA-grafted MNPs.

**Table 3.1** Average size and zeta potential of MNPs measured by DLS.

Sample	Hydrodynamic (nm)	PDI	Zeta potential (mV)
Bare MNPs	318.40±18.21	0.30	-18.0
PAA-grafted MNPs	460.21±20.98	0.37	-31.43
CWBD-conjugated MNPs	626.90±20.12	0.31	-14.40

The presence of organic components of PAA and CWBD on PAA-grafted MNPs and CWBD-conjugated MNPs was further confirmed by TGA. As shown in Figure 3.4, the first weight loss of all MNPs took place at below 200 °C which should be originated from evaporation of water. CWBD-conjugated MNPs shows the highest weight loss of about 3.44%, implying that they contained the greatest of bound water content. The second weight loss occurring in a temperature range of 300-600 °C could be ascribed to the decomposition of organic contents bonded to MNPs. The greater weight loss of 9.13 and 9.80% of PAA-grafted MNPs and CWBD-conjugated MNPs, respectively than that of MNPs (5.47%) confirmed the presence of PAA and CWBD on MNPs. The third weight loss appearing at the highest temperature (>730 °C) in both PAA-grafted MNPs and CWBD-conjugated MNPs should be a contribution of char of macromolecular organic content (PAA and CWBD) on the MNPs because such weight loss was absent in MNPs curve.



**Figure 3.4** TGA (under N<sub>2</sub>) curves of (a) unmodified MNPs, (b) PAA-grafted MNPs, and (c) CWBD-conjugated MNPs analyzed with a heating rate of 20 °C/min.

Molecular weight ( $\overline{M}_n$ ) and functional group of PAA simultaneously formed in solution from the “added” initiator were determined by <sup>1</sup>H NMR analysis. As shown in Figure 3.5, the characteristic <sup>1</sup>H NMR peaks of the methylene proton in the AA unit (–CH(COOH)) and those aromatic protons of the dithiobenzoate group at the chain end of PAA appeared at 2.1–2.3 and 7.2–7.9 ppm, respectively. The average  $M_n$  of PAA was calculated from the relative ratio between the peak integration of protons from the PAA backbone and the peak integration of protons from the dithiobenzoate groups using eqn. 3.1. The fact that the calculated  $M_n$  of 8465 g/mol closely resembled the anticipated value (7206 g/mol) for the target degree of polymerization (DP) of 100 suggested that the RAFT process was well controlled.



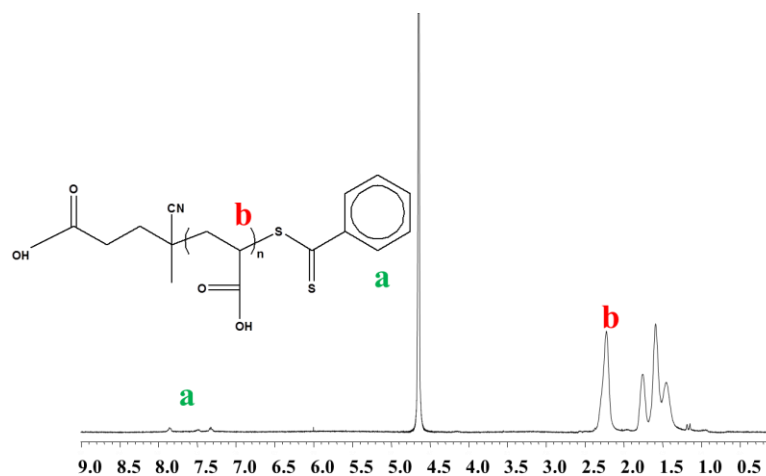


Figure 3.5  $^1\text{H}$  NMR spectrum of PAA in  $\text{D}_2\text{O}$

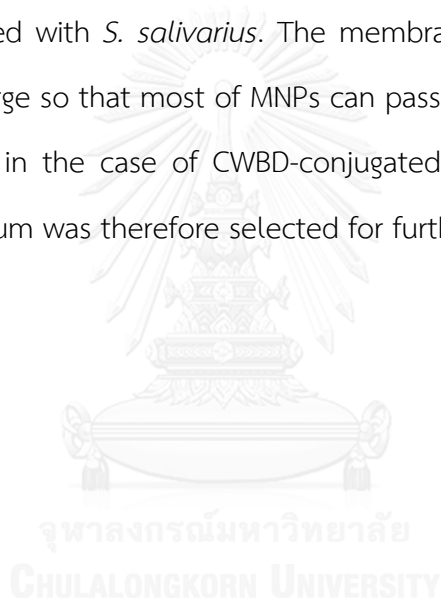
$$\text{Average } M_n = \left\{ \frac{\text{integral of the } H_b \times M_n(\text{acrylic acid})}{\left( \frac{\text{integral of the } H_a}{5} \right)} \right\} + M_n(\text{CTA}) \quad (3.1)$$

$$M_n(\text{acrylic acid}) = 72.06 \text{ g/mol}, M_n(\text{CTA}) = 279.38 \text{ g/mol}$$






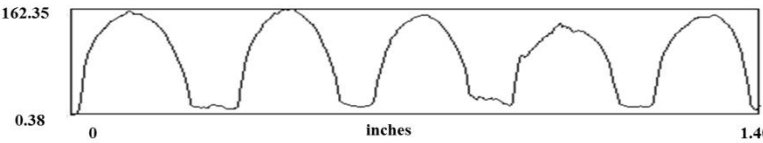





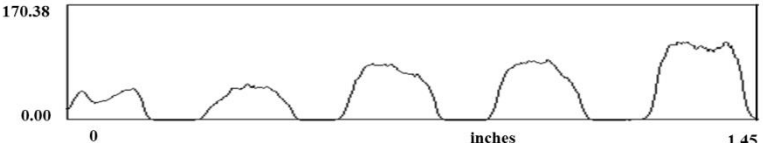





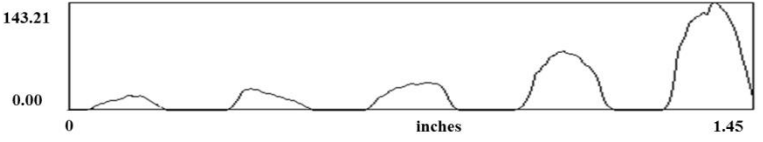





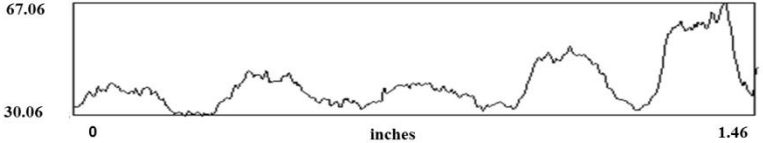
### 3.2 Selection of Filter Membranes Suitable for Selective Filtration Assay

To identify filter membrane with an appropriate pore dimension that can separate CWBD-conjugated MNPs bound with bacteria, selective filtration was performed using filter membranes having varied pore size. As seen in Table 3.2, the pore size of  $0.2 \mu\text{m}$  seems to be too small so that it cannot distinguish the CWBD-conjugated MNPs between before and after capturing both bacteria (*S. mutans* and *S. salivarius*) that are specific to the CWBD. The pore was small so that even the unmodified MNPs cannot go through the membrane so as the PAA-grafted MNPs. This outcome agree well with the dimension of the unmodified MNPs which had a size of approximately  $320 \text{ nm}$  (about  $0.32 \mu\text{m}$ ) as identified by TEM and DLS. Increasing the

pore size to 0.45  $\mu\text{m}$ , the intensity of CWBD-conjugated MNPs on membrane was relatively high regardless of bacteria binding. This is not surprising given that the size of CWBD-conjugated MNPs ( $745.5 \pm 29.9$  and  $626.90 \pm 20.12$  nm as evaluated by TEM and DLS, respectively) is definitely larger than the pore size. And only unmodified and PAA-grafted MNPs can go through the pores. As anticipated, selective filtration worked effectively using the filter membrane with pore size of 0.8  $\mu\text{m}$ . The brown stain was so intense once the CWBD-conjugated MNPs bound with bacteria especially in the case of *S.mutans* implying greater specificity of the CWBD towards *S.mutans* as compared with *S. salivarius*. The membrane with the pore size of 1.2  $\mu\text{m}$  was rather too large so that most of MNPs can pass through the membrane even with bound bacteria in the case of CWBD-conjugated MNPs. The filter membrane with pore size of 0.8  $\mu\text{m}$  was therefore selected for further investigation.



**Table 3.2** Color signal and its corresponding intensity of the spot on the nitrocellulose membrane having varied pore size after filtering MNPs, PAA-grafted MNPs, CWBD-conjugated MNPs both before and after bacteria capturing.

Pore size	MNPs	PAA-MNPs	CWBD-MNPs	<i>S. salivarius</i> -CWBD-MNPs	<i>S. mutans</i> -CWBD-MNPs
<b>0.2 μm</b>					
					
<b>Intensity</b>	132.88	128.73	131.70	119.83	129.92
<b>0.45 μm</b>					
					
<b>Intensity</b>	21.70	81.12	118.60	118.16	120.18
<b>0.8 μm</b>					
					
<b>Intensity</b>	21.70	30.15	40.13	80.54	141.65
<b>1.2 μm</b>					
					
<b>Intensity</b>	10.23	12.74	16.14	23.18	31.84

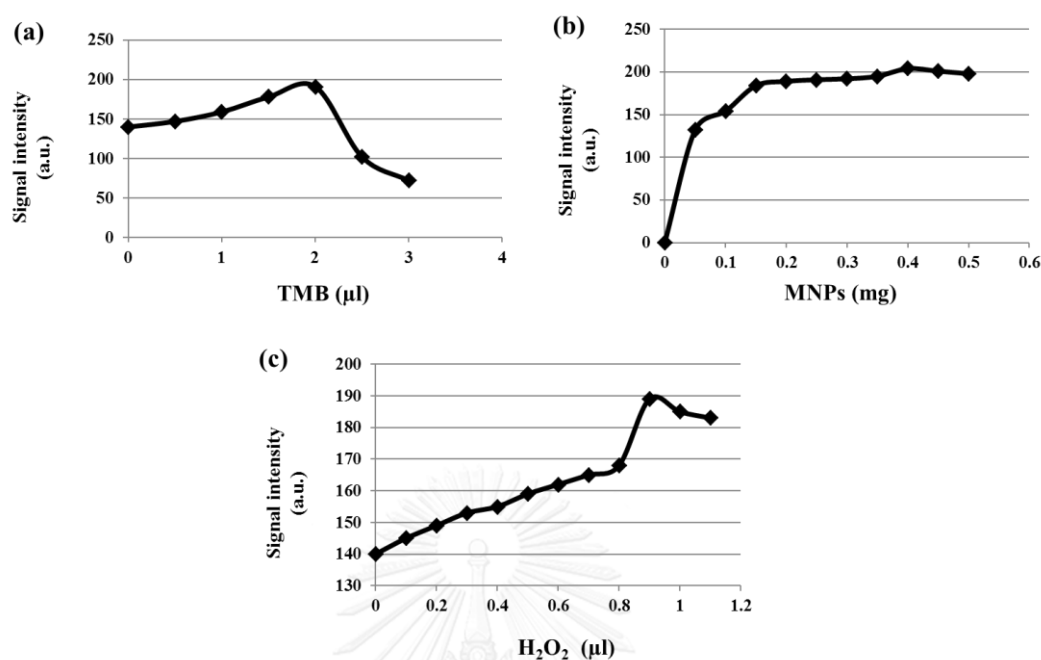
### 3.3 Determination of Peroxidase-like Activity of MNPs

In order to utilize the catalytic activity of MNPs in the oxidative reaction of TMB in the presence of  $H_2O_2$  to develop color reaction, we first tested whether the

catalytic activity of MNPs deposited on filter membrane were dependent on the amount of TMB,  $H_2O_2$  and MNPs as shown in Figure 3.6. To identify an optimal quantity of TMB substrate for oxidation in the presence of  $H_2O_2$ , TMB volume was varied in a range of 0 to 3  $\mu$ L. The result illustrated in Figure 3.6a suggested that the optimal quantity of TMB substrate that gave the highest signal intensity was about 2  $\mu$ L. The intensity of membrane was remarkably decreased when as much as 3  $\mu$ L of TMB was used.

To determine whether the catalytic activity of MNPs was dependent on the amount of MNPs, weight of MNPs was varied from 0 to 0.5 mg. As seen in Figure 3.6b, the results indicated that the peroxidase-like activity of MNPs was dependent on the quantity of MNPs for up to 0.15 mg. Not much further increase in intensity was detected for the MNPs having weight equal and above 0.2 mg. This result suggested that 0.15 mg is certainly adequate to generate highest signal amplification.

In addition, a volume of  $H_2O_2$  was increased up to 1.1  $\mu$ L. The result which can be seen in Figure 3.6c inferred that the intensity increased along with the increase of  $H_2O_2$  from 0 to 0.9  $\mu$ L. The intensity tended to decrease once the amount of  $H_2O_2$  exceeded that value.



**Figure 3.6** The peroxidase-like activity of MNPs to catalyze the color reaction of TMB in the presence of H<sub>2</sub>O<sub>2</sub> which was varied as a function of the amount of (a) TMB substrate, (b) MNPs, and (c) H<sub>2</sub>O<sub>2</sub>.

### 3.4 Determination of Bacteria Binding of CWBD-PAA-MNPs

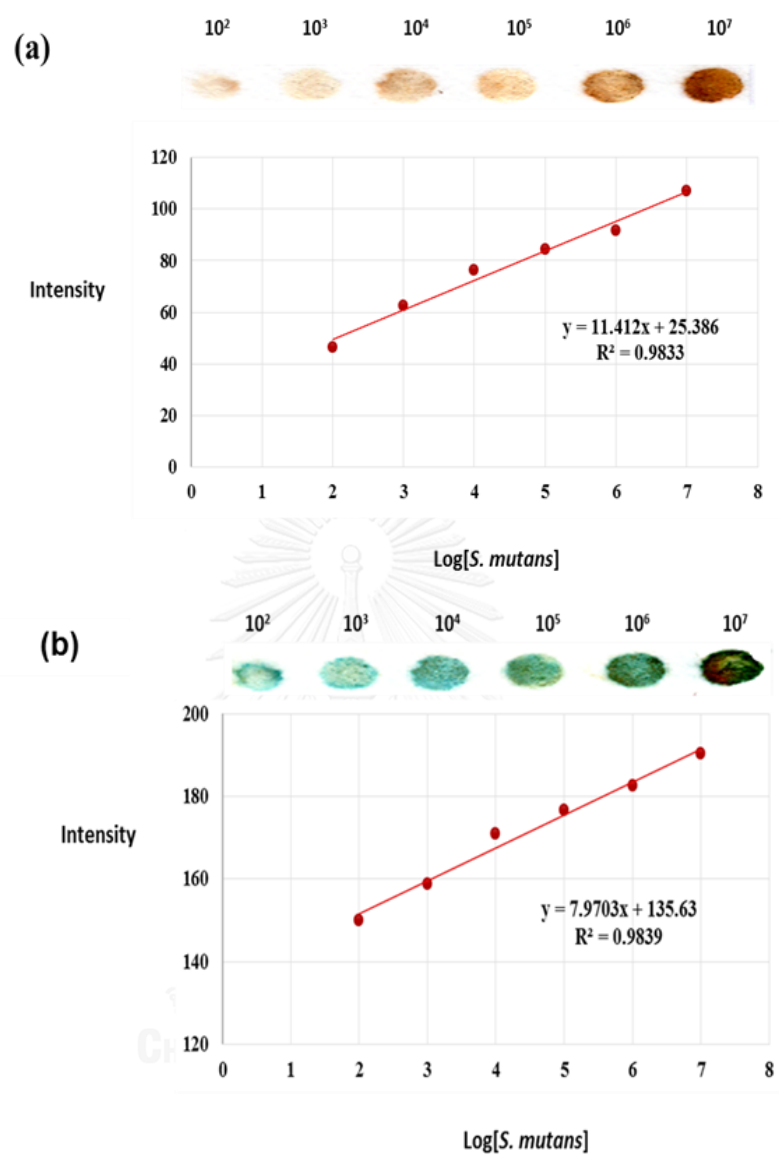
Bacteria binding of the CWBD-PAA-MNPs against two specific bacterial strains, *S. mutans* and *S. sobrinus* having a concentration range of  $1 \times 10^2$  -  $1 \times 10^7$  CFU/mL were determined. Figure 3.7 shows the intensity of the brown spots produced by bacteria bound CWBD-conjugated MNPs on the filter membrane having the pore size of 0.8 μm. The intensity was converted to numeric value to generate a typical standard curve. The intensity of the colored spots increased linearly as a function of log[CFU] of both bacteria (Figure 3.7a-b). Detection limit (LOD) of the method which is the lowest detectable bacterial concentration can be estimated from color intensity at least three times higher than the standard deviation of the background (0 CFU/mL). At 0 CFU/mL, intensity was found to be  $24.81 \pm 5.14$ . LOD which is three

times SD can be calculated as  $2 \times 10^1$  CFU. LOD was calculated by the following equation 3.1.

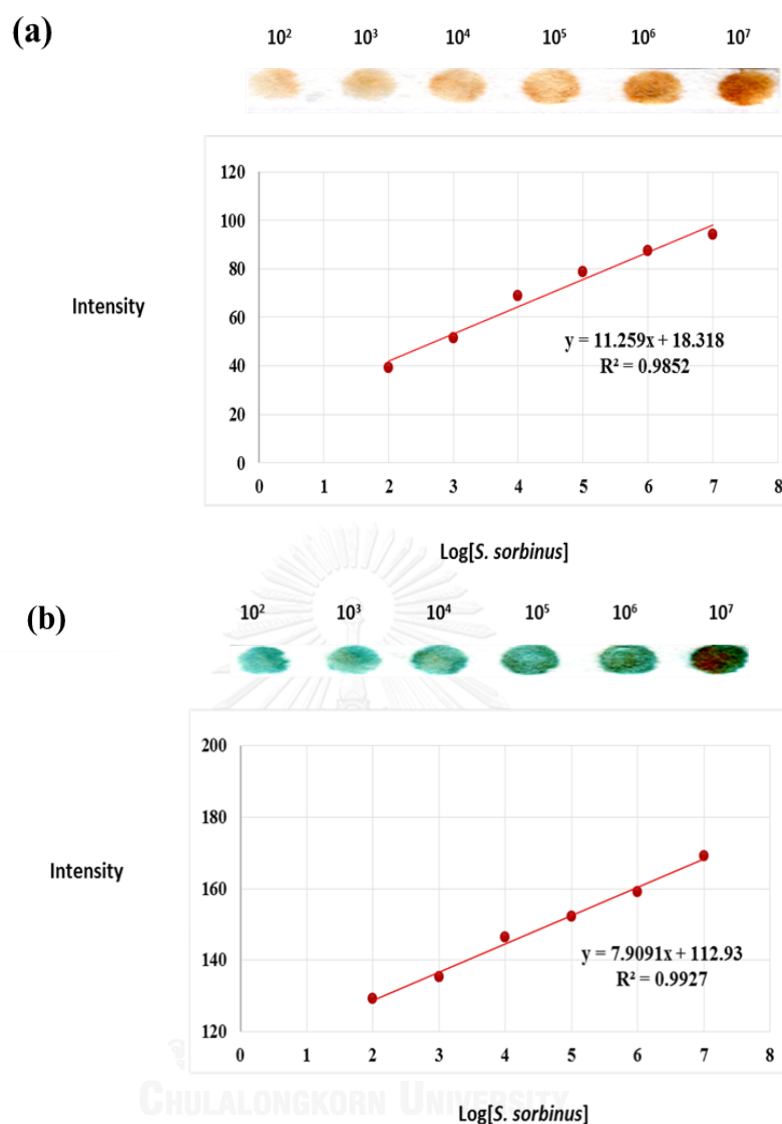
$$I_{LOD} = 3SD_0 + I_0 \quad (3.2)$$

$I_{LOD}$  represents the intensity at LOD whereas  $I_0$  reflects the intensity of the background and  $SD_0$  is standard deviation of the background. After that, LOD was calculated from  $I_{LOD}$  using linear equation of the calibration curve [17].

As shown in Figure 3.7b, after adding TMB and  $H_2O_2$  on bacteria bound CWBD-conjugated MNPs on filter membrane, the membrane turned from brown to blue. The intensity of the membrane also increased linearly as the number of *S. mutans* cells grew exponentially from  $1 \times 10^2$  to  $1 \times 10^7$  CFU/mL. The calculated LOD was found to be 8 CFU/mL. This lower LOD indicated improved sensitivity as a result of signal amplification by peroxidase-like activity of MNPs in the presence of TMB/ $H_2O_2$ . Linear relationship between intensity and log [CFU] was also found for *S. sobrinus* as shown in Figure 3.8.



**Figure 3.7** Linear relationship between log (CFU/mL) and intensity both (a) before and (b) after signal amplification in the presence of TMB/H<sub>2</sub>O<sub>2</sub> for *S. mutans*.



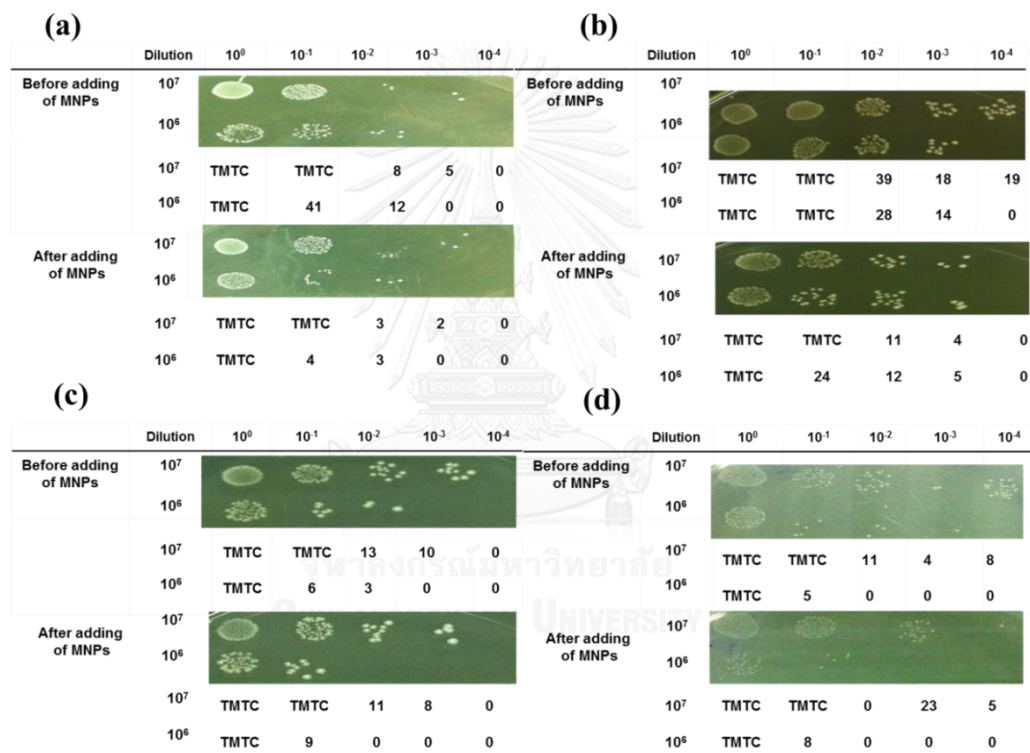
**Figure 3.8** Linear relationship between log (CFU/mL) and intensity both before (a) and after (b) signal amplification in the presence of TMB/H<sub>2</sub>O<sub>2</sub> for *S. sobrinus*.

### 3.5 Determination of Bacteria Capture Efficiency of CWBD-conjugated MNPs

Capture efficiency of the CWBD-conjugated MNPs against target bacteria was determined using bacterial concentration of  $1 \times 10^6$  and  $1 \times 10^7$  CFU/mL. Number of colonies formed on the agar plate was counted both before ( $C_{\text{before}}$ ) and after ( $C_{\text{after}}$ ) the CWBD-conjugated MNPs were added to the bacterial solution upon appropriate dilution.



As can be seen in Figure 3.9a, the number of *S. mutans* colonies appearing on agar plate for both concentrations ( $1 \times 10^6$  and  $1 \times 10^7$  CFU/mL) was decreased after some of them being captured by the CWBD-conjugated MNPs. It should be emphasized that at least 10 times dilution was necessary otherwise there were too many bacteria colonies to count (TMTC). Similar trend was also observed in the case of other bacterial strains but with different capturing ability (Figure 3.9b-d).



TMTC: too many to count

**Figure 3.9** Colonies of (a) *S. mutans*, (b) *S. sobrinus*, (c) *S. salivarius*, and (d) *S. sanguinis* before and after the addition of CWBD-conjugated MNPs.

To be more quantitative, capture efficiencies (CE) can be calculated from those counts using eqn. 3.3.  $C_{\text{before}}$  represents the number of colonies formed on the

agar plate by diluted bacteria stock in PBS whereas  $C_{\text{after}}$  reflects the number of the unbound bacteria after contacting with the CWBD-conjugated MNPs [12]. The capture efficiencies of the CWBD-conjugated MNPs for *S. mutans* and *S. sobrinus* were found to be 77% and 69%, respectively whereas *S. salivarius* and *S. sanguinis* possessed much lower values of 15% and 38%, respectively. These values indicated the specificity of the CWBD-conjugated MNPs towards two specific strains, *S. mutans* and *S. sobrinus*, as opposed to *S. salivarius* and *S. sanguinis*.

$$\text{Capture efficiency (\%)} = \{(C_{\text{before}} - C_{\text{after}}) / C_{\text{before}}\} \times 100 \quad (3.3)$$

This assumption was further verified by monitoring the stained intensity of the CWBD-conjugated MNPs that remain on the filter membrane after contacting with all four bacterial strains. As shown in Figure 3.10, the color intensity values obtained with the untargeted bacteria, *S. salivarius* and *S. sanguinis* were much lower than those detected with *S. mutans* and *S. sobrinus*.

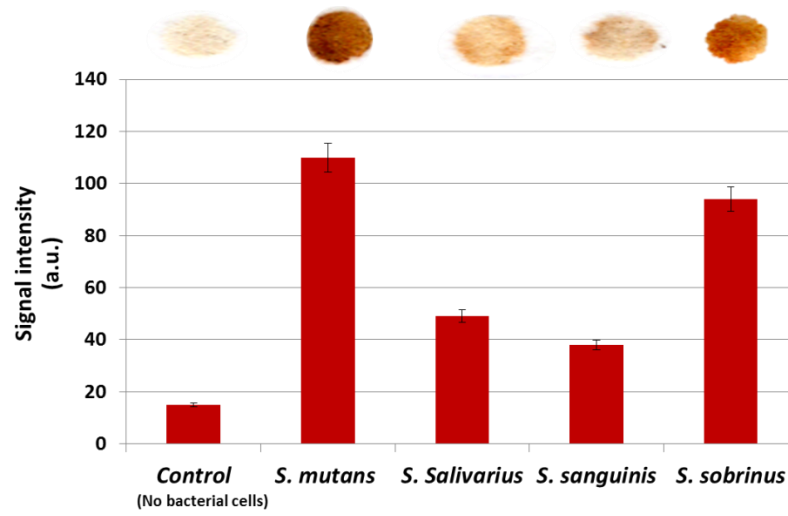


Figure 3.10 Determination of specificity of the CWBD-conjugated MNPs against all bacteria.



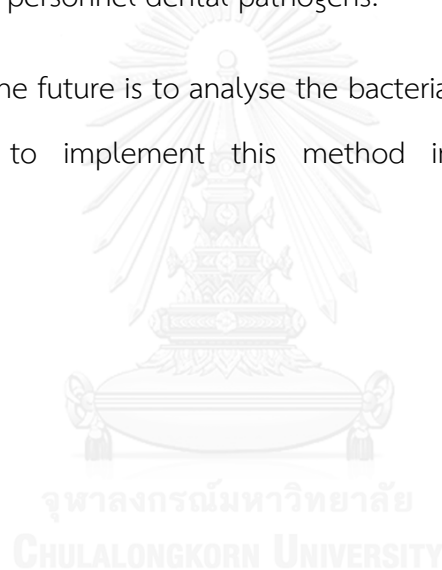
## CHAPTER V

### CONCLUSION AND SUGGESTIONS

The present study has demonstrated that the PAA-grafted MNPs can be prepared by surface-initiated RAFT polymerization. The CWBD of automutanolysin was then conjugated with the PAA-grafted MNPs by EDC/NHS coupling to yield CWBD-conjugated MNPs. The MNPs undergoing PAA grafting and CWBD conjugation were characterized by XRD, FT-IR, TEM, TGA and DLS. The CWBD-conjugated MNPs can be used for the colorimetric detection of mutans streptococci using magnetic separation and selective filtration methods. The nitrocellulose filter membrane with pore size of 0.8  $\mu\text{m}$  was found to be the most suitable substrate for developing the selective filtration for mutans streptococci detection. When bacteria bound CWBD-conjugated MNPs, the size of the complex increase such that it cannot pass through the membrane and then can be colorimetrically measured, while unbound nanocomposites can pass through the membrane. The intensity of the colored spots increased linearly as a function of  $\log[\text{CFU}]$  of both targeted bacteria, *S. mutans* and *S.sobrinus* in a concentration range of  $1 \times 10^2$  -  $1 \times 10^7$  CFU/mL. This allows for semi-quantitative analysis of *S. mutans* from the intensity of MNPs stain left on the membrane and to be able to identify high caries risk case in which bacteria concentration is above  $10^6$  CFU/mL. The specificity of *S. mutans* detection was determined in comparison with the non-targeted bacteria (*S. salivarius* and *S. sanguinis*) ( $1 \times 10^6$  CFU/mL) by monitoring the stained intensity of the CWBD-conjugated MNPs that remain on the filter membrane. The CWBD-conjugated MNPs mixed with *S. mutans* and *S.sobrinus* showed the highest intensity of brown spot on filter membrane whereas those mixed with other streptococci showed less intensity. The capture efficiencies of CWBD-conjugated MNPs for *S. mutans* and *S. sobrinus* were 77 and 69%, respectively, whereas much lower values were achieved for

*S. salivarius* and *S. sanguinis* (15% and 38%, respectively). Addition of TMB and H<sub>2</sub>O<sub>2</sub> on the membrane surface along with the bacteria-bound CWBD-conjugated MNPs can help enhancing the signal. The detection limit of the method for *S. mutans* with and without TMB and H<sub>2</sub>O<sub>2</sub> addition were  $2 \times 10^1$  and 8 CFU/mL, respectively. The assay could be performed within 50 min, yielding results in a similar time period as compared with recently reported antibody immobilized on magnetic particle-based methods. This simple, quick, easy to operate, highly sensitive and specific colorimetric assay is apparently attractive to be further developed into a practical method for detecting personnel dental pathogens.

Our plan for the future is to analyse the bacteria quantity in real sample from human saliva and to implement this method into a real clinical setting.





## REFERENCES

- [1] Anjomshoaa, I., Cooper, M.E., and Vieira, A.R. Caries is associated with asthma and epilepsy. European Journal of Dentistry 3(4) (2009): 297-303.
- [2] Ling, Z. and Tao, H. and Xuedong, Z. Dental Caries. Principles and Management 14(2) (2016): 129-155.
- [3] Bönecker, M., Abanto, J., Tello, G., and Oliveira, L.B. Impact of dental caries on preschool children's quality of life: an update. Brazilian Oral Research 26 (2012): 103-107.
- [4] Sheiham, A. Dental caries affects body weight, growth and quality of life in pre-school children. British Dental Journal 201(10) (2006): 625-626.
- [5] Hurlbutt, M., and Young, D.A. A best practices approach to caries management. Journal of Evidence-Based Dental Practice 14 (2011): 77-86.
- [6] Carounanidy, U. and Sathyanarayanan, R. Dental caries: A complete changeover, PART III: Changeover in the treatment decisions and treatments. Journal of Conservative Dentistry : JCD 13(4) (2010): 209-217.
- [7] Conrads, G., Jiran, S., and Fond, A. Comparing the cariogenic species *Streptococcus sobrinus* and *S. mutans* on whole genome level. Journal of Oral Microbiology 6 (2014): 412-419.
- [8] Gao, X.-L., Seneviratne, C.J., Lo, E.C.M., Chu, C.H., and Samaranayake, L.P. Novel and conventional assays in determining abundance of *Streptococcus mutans* in saliva. International Journal of Paediatric Dentistry 22(5) (2012): 363-368.
- [9] Yoshimura, G. Identification and molecular characterization of an N-acetylmuraminidase, Aml, involved in *Streptococcus mutans* cell separation. Microbiology and Immunology 50(9) (2006): 729-742.
- [10] Wright, D.J., Chapman, P.A., and Siddons, C.A. Immunomagnetic separation as a sensitive method for isolating *Escherichia coli* O157 from food samples. Epidemiology and Infection 113(1) (1994): 31-39.

- [11] Varshney, M., Yang, L., Su, X.-L., and Li, Y. Magnetic nanoparticle-antibody conjugates for the separation of Escherichia coli O157:H7 in ground beef. Journal of Food Protection 68(9) (2005): 1804-1811.
- [12] Shim, W.-B., Lee, C.-W., Kim, M.-G., and Chung, D.-H. An antibody-magnetic nanoparticle conjugate-based selective filtration method for the rapid colorimetric detection of Listeria monocytogenes. Analytical Methods 6(22) (2014): 9129-9135.
- [13] Mine, Y. Separation of salmonella enteritidis from experimentally contaminated liquid eggs using a hen IgY immobilized immunomagnetic separation system. Journal of Agricultural and Food Chemistry 45(10) (1997): 3723-3727.
- [14] Cudjoe, K.S., Hagtvedt, T., and Dainty, R. Immunomagnetic separation of Salmonella from foods and their detection using immunomagnetic particle (IMP)-ELISA. International Journal of Food Microbiology 27(1) (1995): 11-25.
- [15] Gu, H., Xu, K., Xu, C., and Xu, B. Biofunctional magnetic nanoparticles for protein separation and pathogen detection. Chemical Communications (Camb) 5(9) (2006): 941-949.
- [16] Mei, Z., Dhanale, A., Gangaharan, A., Sardar, D.K., and Tang, L. Water dispersion of magnetic nanoparticles with selective Biofunctionality for enhanced plasmonic biosensing. Talanta 151 (2016): 23-29.
- [17] Sung, Y.J., Suk, H.J., Sung, H.Y., Li, T., Poo, H., and Kim, M.G. Novel antibody/gold nanoparticle/magnetic nanoparticle nanocomposites for immunomagnetic separation and rapid colorimetric detection of Staphylococcus aureus in milk. Biosenser Bioelectronics 43 (2013): 432-439.
- [18] Shim, W.B., Song, J.E., Mun, H., Chung, D.H., and Kim, M.G. Rapid colorimetric detection of salmonella typhimurium using a selective filtration technique combined with antibody-magnetic nanoparticle nanocomposites. Analytical and Bioanalytical Chemistry 406(3) (2014): 859-866.
- [19] Cheng, Y., and Seo, M. Combining biofunctional magnetic nanoparticles and ATP bioluminescence for rapid detection of Escherichia coli. Talanta 77(4) (2009): 1332-1336.



- [20] Tümtürk, H., Sahin, F., and Turan, E. Magnetic nanoparticles coated with different shells for biorecognition: high specific binding capacity. Analyst 139(5) (2014): 1093-1100.
- [21] Khalkhali, M. Synthesis and characterization of dextran coated magnetite nanoparticles for diagnostics and therapy. Bioimpacts 5(3) (2015): 141-150.
- [22] Wang, W.-C., Neoh, K.-G., and Kang, E.-T. Surface functionalization of Fe<sub>3</sub>O<sub>4</sub> magnetic nanoparticles via RAFT-mediated graft polymerization. Macromolecular Rapid Communications 27(19) (2006): 1665-1669.
- [23] Ramasamy, M., Zhu, Y., Paik, U., and Yi, D.K. Synthesis and anti-bacterial activity of AuNRs-PS-MNPs. Materials Letters 137 (2014): 479-482.
- [24] Rutnakornpituk, M., Puangsin, N., Theamdee, P., Rutnakornpituk, B., and Wichai, U. Poly(acrylic acid)-grafted magnetic nanoparticle for conjugation with folic acid. Polymer 52(4) (2011): 987-995.
- [25] Padwal, P., Bandyopadhyaya, R., and Mehra, S. Polyacrylic acid-coated iron oxide nanoparticles for targeting drug resistance in mycobacteria. Langmuir 30(50) (2014): 15266-15276.
- [26] Li, H., and Fong, C. Folate-bovine serum albumin functionalized polymeric micelles loaded with superparamagnetic iron oxide nanoparticles for tumor targeting and magnetic resonance imaging. Acta Biomaterialia 15 (2015): 117-126.
- [27] Kadar, E., Batalha, I.L., Fisher, A., and Roque, A.C. The interaction of polymer-coated magnetic nanoparticles with seawater. Science of the Total Environment 487 (2014): 771-777.
- [28] Chen, G., Wu, Z., and Ma, Y. A novel method for preparation of MNP@CS-tethered coenzyme for coupled oxidoreductase system. Journal of Biotechnology 197 (2015): 52-57.
- [29] Eskandari, H. and Naderi-Darehshori, A. Preparation of magnetite/poly(styrene-divinylbenzene) nanoparticles for selective enrichment-determination of fenitrothion in environmental and biological samples. Analytica Chimica Acta 743 (2012): 137-144.

- [30] Qin, S., Wang, L., Zhang, X., and Su, G. Grafting poly(ethylene glycol) monomethacrylate onto Fe<sub>3</sub>O<sub>4</sub> nanoparticles to resist nonspecific protein adsorption. Applied Surface Science 257(3) (2010): 731-735.
- [31] Khoobi, M., and Salad, A. Polyethyleneimine-modified superparamagnetic Fe<sub>3</sub>O<sub>4</sub> nanoparticles: An efficient, reusable and water tolerance nanocatalyst. Journal of Magnetism and Magnetic Materials 375 (2015): 217-226.
- [32] Akbarzadeh, A., Morbez, C., and Corires, B. Synthesis, characterization, and in vitro evaluation of novel polymer-coated magnetic nanoparticles for controlled delivery of doxorubicin. Journal of Nanotechnology, Science and Applications 5 (2012): 13-25.
- [33] Falatach, R., and Sacooli, W. The best of both worlds: active enzymes by grafting-to followed by grafting-from a protein. Chemical Communications (Camb) 51(25) (2015): 5343-5346.
- [34] Mu, B., Wang, T., Wu, Z., Shi, H., Xue, D., and Liu, P. Fabrication of functional block copolymer grafted superparamagnetic nanoparticles for targeted and controlled drug delivery. Colloids and Surfaces A: Physicochemical and Engineering Aspects 375(1-3) (2011): 163-168.
- [35] Fan, X., Lin, L., and Messersmith, P.B. Surface-initiated polymerization from TiO<sub>2</sub> nanoparticle surfaces through a biomimetic initiator: A new route toward polymer-matrix nanocomposites. Composites Science and Technology 66(9) (2006): 1198-1204.
- [36] Lutz, J.-F. Polymerization of oligo(ethylene glycol) (meth)acrylates: Toward new generations of smart biocompatible materials. Journal of Polymer Science Part A: Polymer Chemistry 46(11) (2008): 3459-3470.
- [37] Sahoo, B., Devi, K.S., Banerjee, R., Maiti, T.K., Pramanik, P., and Dhara, D. Thermal and pH responsive polymer-tethered multifunctional magnetic nanoparticles for targeted delivery of anticancer drug. ACS Applied Materials & Interfaces 5(9) (2013): 3884-3893.
- [38] Dutta, S., Parida, S., Maiti, C., Banerjee, R., Mandal, M., and Dhara, D. Polymer grafted magnetic nanoparticles for delivery of anticancer drug at lower pH

- and elevated temperature. Journal of Colloid and Interface Science 467 (2016): 70-80.
- [39] Chiu, Y.C. and Chen, Y.C. Carboxylate-functionalized Iron oxide nanoparticles in surface-assisted laser desorption/ionization mass spectrometry for the analysis of small biomolecules. Analytical Letters 41(2) (2008): 260-267.
- [40] Wang, S., Zhou, Y., Peng, J., Niu, H., Zhang, X., and Yang, F. Surface-induced reversible addition-fragmentation chain-transfer (RAFT) polymerization on magnetic nanoparticles to resist nonspecific adsorption of proteins. Chemical Engineering Journal 173(3) (2011): 873-878.
- [41] Gao, L., Wu, J., Lyle, S., Zehr, K., Cao, L., and Gao, D. Magnetite nanoparticle-linked immunosorbent assay. The Journal of Physical Chemistry C 112(44) (2008): 17357-17361.
- [42] Woo, M.A., Kim, M.I., Jung, J.H., Park, K.S., Seo, T.S., and Park, H.G. A novel colorimetric immunoassay utilizing the peroxidase mimicking activity of magnetic nanoparticles. International Journal of Molecular Sciences 14(5) (2013): 9999-10014.
- [43] Zhang, Z., Wang, Z., Wang, X., and Yang, X. Magnetic nanoparticle-linked colorimetric aptasensor for the detection of thrombin. Sensors and Actuators B: Chemical 147(2) (2010): 428-433.
- [44] Park, J.Y., Jeong, H.Y., Kim, M.I., and Park, T.J. Colorimetric detection system for Salmonella typhimurium based on peroxidase-Like activity of magnetic nanoparticles with DNA aptamers. Journal of Nanomaterials 20 (2015): 1-9.
- [45] Zhuang, J. and Vanza, C. A novel application of iron oxide nanoparticles for detection of hydrogen peroxide in acid rain. Materials Letters 62(24) (2008): 3972-3974.



APPENDIX

จุฬาลงกรณ์มหาวิทยาลัย  
CHULALONGKORN UNIVERSITY

**Table A.1** Amino acid composition of automutanolysin.

Number of amino acids: 748

Molecular weight: 81464.0

Theoretical pI: 5.17

Amino acids	The number of amino acids	% Composition
Ala	73	9.8%
Arg	15	2.0%
Asn	59	7.9%
Asp	55	7.4%
Gln	51	6.8%
Glu	27	3.6%
Gly	42	5.6%
His	17	2.3%
Ile	47	6.3%
Leu	32	4.3%
Lys	44	5.9%
Met	7	0.9%
Phe	8	1.1%
Pro	19	2.5%
Ser	74	9.9%

Amino acids	The number of amino acids	% Composition
Thr	73	9.8%
Trp	12	1.6%
Tyr	36	4.8%
Val	57	7.6%



## VITA

Miss Aemvika Vittayaprasit was born on June 20th, 1991 in Bangkok, Thailand. She graduated with a Bachelor's degree of Science, majoring in Environmental science, Faculty of Science, Chulalongkorn University in 2013. In the same year, she started as a Master Degree student with a major in Program of Petrochemistry and Polymer Science, Faculty of Science, Chulalongkorn University and finished her study in May 2016.

### Proceeding

May 2016; Poster presentation in the 7th Research Symposium on Petrochemical and Materials Technology and The 22th PPC symposium on Petroleum, Petrochemical and Polymer science at Queen Sirikit National Convention Center, Thailand.

### Patent

1. พนิดา ฉัญญศรีสังข์, เอมวิกา วิทยาประสิทธิ์, วรวิรุ โสเว่น เรื่อง “กรรมวิธีการเตรียมสารประกอบอนุภาคที่สามารถจับกับเชื้อก่อโรคฟันพุได้อย่างจำเพาะสำหรับการแยกและตรวจวัดเชื้อก่อโรคฟันพุเชิงกึ่งปริมาณได้ด้วยตาเปล่า” สิทธิบัตรเลขที่คำขอ 1601003554 วันยื่นคำขอ 16 มิ.ย.2559
2. พนิดา ฉัญญศรีสังข์, เอมวิกา วิทยาประสิทธิ์, วรวิรุ โสเว่น เรื่อง “สารประกอบอนุภาคที่สามารถจับกับเชื้อก่อโรคฟันพุได้อย่างจำเพาะสำหรับการแยกและตรวจวัดเชื้อก่อโรคฟันพุเชิงกึ่งปริมาณได้ด้วยตาเปล่า” อนุสิทธิบัตรเลขที่คำขอ 1603001055 วันยื่นคำขอ 16 มิ.ย.2559